Electronic-structure calculations for amorphous solids using the recursion method and linear muffin-tin orbitals: Application to $Fe_{80}B_{20}$

H. J. Nowak,* O. K. Andersen, T. Fujiwara,† and O. Jepsen
Max-Planck-Institut für Festkörperforschung, Heisenbergstrasse 1, D-7000 Stuttgart 80, Federal Republic of Germany

P. Vargas
Universidad de Santiago de Chile, Departamento de Física, P.O. Box 307, Santiago-2, Chile
(Received 22 January 1991)

We describe a method for performing density-functional calculations for topologically disordered condensed matter. This method combines the recursion and the linear-muffin-tin-orbital (LMTO) methods, and uses the tight-binding representation. In the present version, the LMTO matrix elements are evaluated in the atomic-sphere approximation (ASA). Various levels of approximation for the ASA Hamiltonian, such as the two-center tight-binding one, are systematically derived and tested. The method is applied to crystalline bcc Fe and to amorphous $Fe_{80}B_{20}$. Charge self-consistency is only treated for the average Fe and the average B atoms. The Fe–B bonding is found to be covalent. A Stoner theory is derived and used to describe the ferromagnetism. The structures of our density of states for ferromagnetic $Fe_{80}B_{20}$ agree in detail with reliable photoemission data.

I. INTRODUCTION

In order to calculate the electronic structure of topologically disordered solids and liquids it is customary to solve the one-electron Schrödinger equation with an iterative, real-space scheme and to obtain local quantities such as orbital-projected densities of states. This local point of view has been extensively discussed by Heine, Bullett, Haydock, and Kelly,[1] who advocate the recursion method[2] as the most efficient real-space scheme. Other schemes include the moment method[3] and the cluster-Bethe-lattice method.[4] Common for all schemes is that they require a basis, $|\underline{\chi}\rangle$, of localized orbitals. In order to carry the iteration to reasonable convergence one must include several hundreds of atoms, and this is possible only when the basis is well *localized and minimal*; e.g., it has near-neighbor range and includes only one s, three p, five d, and, possibly, seven f orbitals per atom.

For the calculation of charge transfers, magnetic moments, and interatomic forces using the density-functional formalism, self-consistency of the charge and spin density is usually needed. In such cases it is not sufficient to specify the elements

$$\mathcal{H}_{RL,R'L'} \equiv \langle \chi_{RL}| -\Delta + V(\mathbf{r})|\chi_{R'L'}\rangle \tag{1}$$

and

$$\mathcal{O}_{RL,R'L'} \equiv \langle \chi_{RL}|\chi_{R'L'}\rangle \tag{2}$$

of the one-electron Hamiltonian and overlap matrices, rather, the real-space behavior of the orbitals, i.e., their explicit $\mathbf{r}$ dependence, must be known. Furthermore, the orbitals must form a reasonably complete set for the valence electrons. In (1) and (2), R and L denote the site and the angular-momentum character of the orbital.

With the recursion method a complication arises because the recursion is carried out with a matrix which is either $\mathcal{O}^{-1}\mathcal{H}$, or $\mathcal{O}^{-1/2}\mathcal{H}\mathcal{O}^{-1/2}$, and this matrix must, in practice, be truncated to near-neighbor interactions. This is normally an uncontrolled approximation because short range of the orbitals merely ensures short range of the Hamiltonian and overlap matrices, and not of $\mathcal{O}^{-1}\mathcal{H}$. Similarly, the matrix $\mathcal{O}^{-1/2}\mathcal{H}\mathcal{O}^{-1/2}$ is the Hamiltonian in the basis of Löwdin-orthonormalized orbitals which have fairly long-ranged oscillations. A further complication arises from the fact that the valence-charge density at a given atom originates not only from the orbitals at that site but also from the overlapping orbitals from the neighboring sites and, hence, not only on-site but also off-site elements of the density matrix in the orbital representation are usually needed. However, a recursion calculation merely yields a diagonal element of the density matrix, and, in order to obtain the off-site elements, it is therefore necessary to perform recursions using not only atom-centered orbitals as initial states but also a large number of bonding and antibonding linear combinations.

In this paper we explain and demonstrate how first-principles electronic-structure calculations with the recursion method may conveniently be carried out using a basis of linear muffin-tin orbitals[5] (LMTO's) in a tight-binding (TB) representation.[6–9]

As is well known, the LMTO set is a minimal basis, in the sense mentioned above, and it is complete for the muffin-tin or atomic-sphere potential used for its construction and over an energy range of about one Rydberg. We shall perform the recursion using the Hamiltonian in the Löwdin-orthonormalized representation, $\mathcal{O}^{-1/2}\mathcal{H}\mathcal{O}^{-1/2}$, that is, we shall use the long-ranged orthonormal—rather than the TB—representation. The

long range causes no problems because the effect of truncating the range of the Hamiltonian is controlled in the following way: In the LMTO formalism, $\mathcal{O}^{-1/2}\mathcal{H}\mathcal{O}^{-1/2}$ may be expressed as a power series of a matrix, $h \equiv H - \varepsilon_\nu$, where H is an effective, two-center TB Hamiltonian and ε_ν is an arbitrary energy (diagonal matrix) chosen at the center of interest. If this power series is truncated after the first-order term and, hence, the orthonormal Hamiltonian is approximated by the two-center TB Hamiltonian, the recursion yields a density of states (DOS) whose features have energy positions correct to first order in their distance from ε_ν. If, on the other hand, the truncation is performed after the second-order term the range is twice that of the two-center TB Hamiltonian and the resulting DOS features will have positions correct to second order in their distance from ε_ν, and so on. The fact that the spectrum of such a truncated Hamiltonian is distorted far away from ε_ν is not merely a disadvantage but may even be exploited: Since the energy resolution obtained by recursion to a given level is inversely proportional to the band width, the resolution may be increased if the recursion can be carried out with a Hamiltonian whose spectrum is compressed outside the region of interest. Such a truncated Hamiltonian can usually be found by suitable choice of the TB representation.

With a basis of LMTO's it is not necessary to calculate off-site elements of the density matrix provided that the so-called atomic-sphere approximation (ASA) is used. This is so, because in the ASA the eigenvalue problem for the Hamiltonian matrix is equivalent with a tail-cancellation condition for the orbitals [the Korringa-Kohn-Rostoker (KKR) condition] and, as a consequence, the imaginary part of the Green's function can be expressed as one-center expansions which merely need on-site elements of the density matrix.[10]

A preliminary version of the recursion-TB-LMTO method was applied by one of us to crystalline bcc Fe, to amorphous Fe, to amorphous $Fe_{80}B_{20}$, and to amorphous Cu_xZr_{1-x} alloys.[11] For the two latter amorphous solids, models with about 1500 atoms were used and the recursion was terminated according to the prescription of Beer and Pettifor.[12] Charge self-consistency was achieved for the average Fe and for the average B spheres, and the on-site structure constants of the two-center TB Hamiltonian were approximated by site-independent interpolations between the values obtained for the fcc and bcc structures. The method in its present form has been applied recently to amorphous Si,[13] Ca_7Al_3 glass,[14] amorphous Pd,[15] and to study the possibility of calculating electric-field gradients with recursion.[16]

The paper is organized as follows. In Sec. II we first review those features of the TB-LMTO method which are important for its application to recursion. Then we discuss in detail how the charge density may be obtained. Finally, the recursion method is briefly reviewed and a new terminator is introduced. In Sec. III we compare recursion with band calculation for bcc Fe. As a preliminary to discussing the electronic structure, chemical binding, and ferromagnetism of amorphous $Fe_{80}B_{20}$, we present in Sec. IV a band calculation for the crystal Fe_2B. At the end of this section we develop a Stoner theory appropriate for treating the ferromagnetism of Fe_xB_{1-x}. In Sec. V we then present and discuss our results for amorphous $Fe_{80}B_{20}$. First, we demonstrate the application of our method at various levels of sophistication. Then, we use the most accurate results to make comparisons with experiments, and to discuss the chemical binding and the ferromagnetic electronic structure. Finally, in Sec. VI we conclude.

II. METHOD

The recursion method as well as the solid-state LMTO method have been described in detail elsewhere. In the present section we shall state and explain the results needed in order to apply the recursion method with LMTO's. We start considering the LMTO formalism and then we give a brief account of the recursion method and introduce a linear terminator.

A. Structure constants

In solids and liquids the (classical) kinetic energy of the valence electrons between the atoms is close to zero, and LMTO's are therefore, most simply, chosen to have *envelope functions* which are solutions of the Laplace equation. A conventional solid-state LMTO, $\chi^0_{RL}(\mathbf{r}-\mathbf{R})$, thus has an envelope function proportional to the 2^ℓ-pole field $|\mathbf{r}-\mathbf{R}|^{-\ell-1}Y_L(\mathbf{r}-\mathbf{R})$. If $\mathbf{R}$ takes the values of all the sites in the the solid and if L takes the 4 (*sp*), the 9 (*spd*), or the 16 (*spdf*), angular-momentum values, we obtain the *set of conventional LMTO's*, $|\chi^0\rangle$. This set may be linearly transformed into an equivalent *set of screened LMTO's*, $|\chi^\alpha\rangle$. The envelope of the screened LMTO, $\chi^\alpha_{RL}(\mathbf{r}-\mathbf{R})$, has 2^ℓ-pole character near $\mathbf{R}$ but, in addition, it has screening poles at the neighboring sites. Each set of screened LMTO's is characterized by a set α of *screening constants*, $\alpha_{R\ell}$, and these may, for instance, be determined so as to give the LMTO set short range, or so as to make it nearly orthonormal. For the conventional set, the screening constants are zero. The following two, site-independent sets of screening constants

$$\begin{aligned}\underline{\alpha} &= \{\alpha_s, \alpha_p, \alpha_{\ell>1}\} \\ &= \{0.28723, 0.02582, 0.0\} \equiv \underline{\alpha}_{\mathrm{I}},\end{aligned} \tag{3}$$

for *sp* screening and

$$\begin{aligned}\underline{\alpha} &= \{\alpha_s, \alpha_p, \alpha_d, \alpha_{\ell>2}\} \\ &= \{0.34850, 0.05303, 0.01071, 0.0\} \equiv \underline{\alpha}_{\mathrm{II}}\end{aligned} \tag{4}$$

for *spd* screening have been found numerically[6,7,9,17] to give short-ranged envelope functions for all, reasonably homogeneous, three-dimensional structures. The corresponding LMTO sets are referred to as *tight-binding* sets.[18]

The envelope of $\chi^\alpha_{RL}(\mathbf{r}-\mathbf{R})$ may be expanded about the site $\mathbf{R}'$ in a spherical-harmonics series and the expansion coefficients $S^\alpha_{R'L',RL}$ are the so-called *screened structure constants*. For a given $\underline{\alpha}$, they form a Hermitian matrix which will turn out to be the structural factor of the two-center Hamiltonian for the LMTO set.

The conventional structure constants have the following off-site elements:

$$S^0_{ss\sigma} = -2(w/d), \quad S^0_{sp\sigma} = (2\sqrt{3})(w/d)^2,$$
$$S^0_{pp\{\sigma,\pi\}} = 6\{2,-1\}(w/d)^3, \quad S^0_{sd\sigma} = -(2\sqrt{5})(w/d)^3,$$
$$S^0_{pd\{\sigma,\pi\}} = (6\sqrt{5})\{-\sqrt{3},1\}(w/d)^4, \tag{5}$$
$$S^0_{dd\{\sigma,\pi,\delta\}} = 10\{-6,4,-1\}(w/d)^5, \ldots,$$

where the z axis is chosen along $\mathbf{R}-\mathbf{R}'$ and $d \equiv |\mathbf{R}-\mathbf{R}'|$ is the interatomic distance. A length w is introduced to make the structure constants dimensionless. In order to turn the z axis away from $\mathbf{R}-\mathbf{R}'$ one may use Table I in Ref. 19. Alternatively, one may use the table given in Ref. 5, or the general formula, given in the same reference, valid for any z direction and for any L and L'. The on-site elements of the conventional structure constants vanish per definition.

The screened structure constants are given in terms of the conventional ones and the screening constants by the "Dyson equation:"

$$S^\alpha_{RL,R'L'} = S^0_{RL,R'L'} + \sum_{R'',L''} S^\alpha_{RL,R''L''}\alpha_{R''\ell''}S^0_{R''L'',R'L'}, \tag{6}$$

or, in matrix notation,

$$S^\alpha = S^0(1-\alpha S^0)^{-1} = \alpha^{-1}[(\alpha^{-1}-S^0)^{-1}-\alpha]\alpha^{-1}, \tag{7}$$

where α is considered a diagonal matrix with elements $\alpha_{R\ell}$.

If α is given by Eq. (3) or Eq. (4), and if the length w entering the definition of S^0 is taken to be the average Wigner-Seitz radius, i.e., if

$$(4\pi/3)w^3 \equiv V_{\text{site}}, \tag{8}$$

where V_{site} is the volume per site, then the screened structure constants are so localized that they effectively vanish when the interatomic distance d exceeds the radius of a cluster containing about 20 atoms for *spd* screening and about 50 atoms for *sp* screening. These structure constants are named the *tight-binding structure constants* S^α. The choice (8) for w is indeed not crucial; for instance, the structure constants with $\underline{\alpha} \equiv \underline{\alpha}_{\text{I}}$ or $\underline{\alpha}_{\text{II}}$ are well localized, even for the extremely inhomogeneous structure consisting of a surface of a semi-infinite solid when w is taken to be the Wigner-Seitz radius of the bulk.[17] For an amorphous system one could thus calculate the tight-binding structure constants by inverting, for each site, the Hermitian, positive-definite matrix $\alpha^{-1}-S^0$ in (7) for the cluster centered at that site. The dimension of the square matrix to be inverted is approximately 20×9 for *spd* screening and 50×4 for *sp* screening, that is, about 200.

The *off-site* elements of the tight-binding structure constants, which will turn out to be the structural factors of the "hopping integrals," follow the universal interpolation formula[17]

$$S^\alpha_{\ell\ell'm} = A^\alpha_{\ell\ell'm}\exp(-\lambda^\alpha_{\ell\ell'm}d/w) \tag{9}$$

rather closely, provided that the distribution of sites within a distance of order $10w/\lambda$ is reasonably homogeneous and that w is taken to be the local average Wigner-Seitz radius. The parameters A and λ are given in Table I, and we see that the screening set $\underline{\alpha}_{\text{II}}$, which includes quadrupole screening (s,p,d), gives a somewhat shorter range ($\lambda \approx 3.5$) than the set $\underline{\alpha}_{\text{I}}$ ($\lambda \approx 2.5$), which includes screening with monopoles and dipoles only. On the other hand, if quadrupole screening is included, the LMTO basis set must (usually) include the d orbitals in order to be reasonably complete, regardless of whether there are d states or not in the energy range of interest. Similarly, if one is willing to always include the f orbitals, a set $\underline{\alpha}_{\text{III}}$, slightly more localized than $\underline{\alpha}_{\text{II}}$, could be used. The *on-site* elements of the tight-binding structure constants do not vanish. They depend sensitively on the local environment and have no approximation in terms of a simple, structure-independent interpolation formula. This will be shown by the example of

TABLE I. Parameters of the interpolation formula $S^\alpha_{\ell\ell'm} = Ae^{-\lambda d/w}$ for the off-site elements of the TB structure constants. We have used *sp* screening (set I) and *spd* screening (set II). The screening constants $\underline{\alpha}_{\text{I}}$ and $\underline{\alpha}_{\text{II}}$ are given by Eqs. (3) and (4), respectively. w is the average Wigner-Seitz radius given by (8). From Refs. 9 and 17.

	spd screening		*sp* screening	
	A_{II}	λ_{II}	A_{I}	λ_{I}
$ss\sigma$	−184.7	3.293	−43.57	2.559
$sp\sigma$	371.7	3.301	81.77	2.503
$pp\sigma$	791	3.331	182.7	2.529
$sd\sigma$	−575	3.440	−84.51	2.444
$pd\sigma$	−1422	3.535	−288.6	2.671
$dd\sigma$	−3685	3.905	−1018	3.199
$pp\pi$	−359.9	3.935	−241.5	3.589
$pd\pi$	837	3.965	487.6	3.558
$dd\pi$	1997	3.998	1272	3.657
$dd\delta$	−844	4.708	−821	4.494

amorphous $Fe_{80}B_{20}$. These "crystal-field" elements are, however, given *explicitly* in terms of the off-site elements by the Dyson equation (6): Since S^0 has no on-site elements, only the off-site elements of S^α appear on the right-hand side of Eq. (6). A simple approximation for the on-site elements of a tight-binding structure matrix is thus obtained by using Eq. (6), together with Eq. (5) for S^0 and the approximation (9) for the tight-binding hopping integrals, S^α.

B. LMTO's and the two-center Hamiltonian

Given an envelope function, the LMTO is now constructed by *continuous and differentiable augmentation inside certain muffin-tin or atomic spheres* with functions, $\varphi_{RL}(\mathbf{r}-\mathbf{R})$ and $\dot{\varphi}^\alpha_{R'L'}(\mathbf{r}-\mathbf{R}')$, to be specified later. We may thus write

$$\chi^\alpha_{RL}(\mathbf{r}-\mathbf{R}) = \kappa^\alpha_{RL}(\mathbf{r}-\mathbf{R}) + \varphi_{RL}(\mathbf{r}-\mathbf{R}) + \sum_{R',L'} \dot{\varphi}^\alpha_{R'L'}(\mathbf{r}-\mathbf{R}')h^\alpha_{R'L',RL},$$

where $\kappa^\alpha_{RL}(\mathbf{r}-\mathbf{R})$ is the envelope function truncated *inside* all spheres[20] and the φ and $\dot{\varphi}$ functions are truncated *outside* their respective spheres. In shorthand matrix notation we express the α *set* of LMTO's as,

$$|\underline{\chi}^\alpha\rangle = |\underline{\kappa}^\alpha\rangle + |\underline{\varphi}\rangle + |\underline{\dot{\varphi}}^\alpha\rangle h^\alpha, \tag{10}$$

where, for instance, $\langle\mathbf{r}|\underline{\varphi}\rangle$ is a row vector with element $\langle\mathbf{r}|\varphi_{RL}\rangle \equiv \varphi_{RL}(\mathbf{r}-\mathbf{R})$, and $\langle\varphi|\mathbf{r}\rangle$ is a column vector with elements $\langle\varphi_{RL}|\mathbf{r}\rangle \equiv \varphi^*_{RL}(\mathbf{r}-\mathbf{R})$, and where h^α is a matrix. Equation (10), crudely speaking, says that the "head" of the envelope is given the proper atomic wiggles through smooth augmentation with a φ function, plus a $\dot{\varphi}$ function times the on-site element of h^α, and that the "tail" of the envelope is orthogonalized to the core states of the neighboring atoms through smooth augmentation with $\dot{\varphi}$ functions. The latter are constructed in such a way that, when multiplied with the proper coefficients h^α, they smoothly match onto the envelope function. This means that the $\dot{\varphi}$ functions by construction must have the proper radial logarithmic derivative at the sphere boundary, and that the coefficients h^α are determined by the condition of continuity of the orbital. They are given by

$$H^\alpha_{RL,R'L'} \equiv \varepsilon_{\nu R\ell}\delta_{RR'}\delta_{LL'} + h^\alpha_{RL,R'L'} = c^\alpha_{R\ell}\delta_{RR'}\delta_{LL'} + \sqrt{d^\alpha_{R\ell}}S^\alpha_{RL,R'L'}\sqrt{d^\alpha_{R'\ell'}}, \tag{11}$$

in terms of the structure constants and certain potential parameters, $\underline{c}^\alpha - \underline{\varepsilon}_\nu$ and $\underline{d}^\alpha$, which depend on the values of φ and $\dot{\varphi}$ at the sphere boundary, and which will be given in Eqs. (16) and (17) below. The Hermitian matrix defined by Eq. (11) will turn out to be the *first-order Hamiltonian* in the atomic-sphere approximation (ASA) (in atomic Rydberg units); it is seen to have the *two-center* form.

C. Augmentation functions and potential parameters

The augmentation functions φ and $\dot{\varphi}$ for a given muffin tin or atomic sphere of radius s_R are obtained from the spherical average, $v_R(|\mathbf{r}-\mathbf{R}|)$, of the potential $V(\mathbf{r})$ by solution of the corresponding radial Schrödinger equations at some chosen energies $\varepsilon_{\nu R\ell}$ and at the neighboring ones $\varepsilon_{\nu R\ell} + d\varepsilon$. Specifically, if $\varphi_{R\ell}(\varepsilon, r)$ is the solution of the ℓth radial Schrödinger equation, normalized to unity in the sphere,

$$\int_0^{s_R} \varphi_{R\ell}(\varepsilon, r)^2 r^2 dr \equiv \langle\varphi_{RL}(\varepsilon)^2\rangle = 1, \tag{12}$$

then the augmentation-function φ is defined by

$$\varphi_{R\ell}(r) \equiv \varphi_{R\ell}(\varepsilon_{\nu R\ell}, r),$$

and the energy-derivative function,

$$\left.\frac{\partial\varphi_{R\ell}(\varepsilon, r)}{\partial\varepsilon}\right|_{\varepsilon_{\nu R\ell}} \equiv \dot{\varphi}^\gamma_{R\ell}(r),$$

is seen to be orthogonal to φ in the sphere. The augmentation-function $\dot{\varphi}$ for the $\underline{\alpha}$ *set* is now defined as follows:

$$\dot{\varphi}^\alpha(r) \equiv \dot{\varphi}^\gamma(r) + \varphi(r)o^\alpha = \left.\frac{\partial\{[1+(\varepsilon-\varepsilon_\nu)o^\alpha]\varphi(\varepsilon, r)\}}{\partial\varepsilon}\right|_{\varepsilon_\nu}, \tag{13}$$

with the constant o^α determined, in Eq. (18) below, to give $\dot{\varphi}$ the same radial logarithmic derivative at the sphere as the envelope tails, i.e.,

$$D\{\dot{\varphi}^\alpha(s)\} \equiv \left.\frac{\partial \ln|\dot{\varphi}^\alpha(r)|}{\partial \ln r}\right|_s = D((s/w)^{-\ell-1} - (s/w)^\ell\alpha/[2(2\ell+1)]) \equiv D^\alpha(s). \tag{14}$$

The definition of $D^\alpha(s)$ is seen to be equivalent to

$$\frac{(s/w)^{2\ell+1}}{2(2\ell+1)}\frac{D^\alpha(s)-\ell}{D^\alpha(s)+\ell+1} = \alpha\,. \tag{15}$$

For simplicity, we have dropped the subscripts $R\ell$ from Eq. (13) and onwards.

The *position- and width-potential parameters* $c^\alpha_{R\ell}$ and $d^\alpha_{R\ell}$, which enter the definition (11) of the two-center, first-order Hamiltonian, may be expressed in terms of the value and the radial logarithmic derivative of φ at the sphere boundary as follows:

$$c^\alpha = \varepsilon_\nu + s[\varphi(s)]^2\frac{[D(\varphi(s))+\ell+1][D^\alpha(s)-D(\varphi(s))]}{D^\alpha(s)+\ell+1} \tag{16}$$

and

$$(d^\alpha)^{1/2} = (s/2)^{1/2}(s/w)^{\ell+1/2}\varphi(s)\frac{D^\alpha(s)-D(\varphi(s))}{D^\alpha(s)+\ell+1}. \tag{17}$$

It is the existence of a Wronskian relation between φ and $\dot{\varphi}$ which makes it possible to evaluate the two-center, first-order Hamiltonian without calculation of $\dot{\varphi}$. This means, for instance, that a rough estimate of this Hamiltonian may be obtained merely from atomic orbitals, chosing the $\varepsilon_{\nu R\ell}$'s as the atomic energies and the $\varphi_{R\ell}(r)$'s as the atomic orbitals renormalized to the spheres. This estimate corresponds to taking the potentials in the spheres as truncated atomic potentials. More realistic estimates of the position parameters, the c's, can be obtained by including the overlap of the neighboring atomic potentials as a perturbation.

The potential parameter needed to specify $\dot{\varphi}$ in (13) is the so-called *overlap parameter*,

$$o^\alpha = \langle \dot{\varphi}^\alpha | \varphi \rangle = \left(s\varphi(s)^2 \frac{[D(\varphi(s)) - D^\alpha(s)][D(\dot{\varphi}^\gamma(s)) - D(\varphi(s))]}{D(\dot{\varphi}^\gamma(s)) - D^\alpha(s)} \right)^{-1}, \tag{18}$$

which depends on the potential parameters $\varphi(s)$, $D(\varphi(s))$, and $D(\dot{\varphi}^\gamma(s))$. Another meaning of this overlap parameter is that $\varepsilon_{\nu R\ell} + 1/o^\alpha_{R\ell}$ is the energy for which the LMTO tails alone solve Schrödinger's equation inside the sphere at R for the angular momentum ℓ, i.e., it is the energy where $D^\alpha_{R\ell}(s) = D(\varphi_{R\ell}(\varepsilon, s))$. If, for a given $R\ell$, this energy lies inside the range of interest, that is within half a Rydberg from $\varepsilon_{\nu R\ell}$ or so (i.e., if $o^\alpha_{R\ell} > 2\ \mathrm{Ry}^{-1}$), then the LMTO's for that sphere and angular momentum can usually be deleted from the basis set because the tails of the other LMTO's suffice to solve Schrödinger's equation throughout the energy range of interest. If these orbitals are *not* deleted, so-called ghost bands might occur. In those rare cases where not only $\varepsilon_{\nu R\ell} + 1/o^\alpha_{R\ell}$ but also $c^\alpha_{R\ell}$ lie inside the range of interest, and, consequently, the $R\ell$ LMTO's cannot be deleted, it may be necessary to change the representation, e.g., from the $\underline{\alpha}_{\mathrm{II}}$ to the $\underline{\alpha}_{\mathrm{I}}$ representation.[18]

As an example, we give in Table II the potential parameters for bcc Fe whose band structure we shall consider in Sec. III. The potential parameters depend on the scale constant w through the definition (15) of $D^\alpha(s)$. The width parameter d^α, according to (17), also contains the factor $(s/w)^{2\ell+1}$.

D. Hamiltonian and overlap matrices

For the LMTO basis of Eq. (10) one finds the following expression for the *overlap matrix*:

$$\mathcal{O} \equiv \langle \underline{\chi} | \underline{\chi} \rangle = (1 + ho)(1 + oh) + hph + \langle \underline{\kappa} | \underline{\kappa} \rangle. \tag{19}$$

Here, and in the following, we drop the superscripts α when the equation holds for a general α. We have, furthermore, used matrix notation with 1 being the unit matrix and with the potential parameters o and p being diagonal matrices with elements $o_{R\ell}$ and

$$p_{R\ell} \equiv \int_0^{s_R} \dot{\varphi}^\gamma_{R\ell}(r)^2 r^2 dr \equiv \langle (\dot{\varphi}^\gamma_{RL})^2 \rangle,$$

respectively. The potential parameters p are the small parameters of a linear method and $\varepsilon_{\nu R\ell} \pm \frac{1}{2}(p_{R\ell})^{-1/2}$ are the "energy windows" inside which such a method can be expected to yield useful results. The widths of these windows are usually several Rydbergs. The last term in Eq. (19) is the integral over the product of two envelope functions in the interstitial region. This integral may be calculated analytically for the conventional, unscreened envelopes, and the transformation to a tight-binding representation then requires left and right multiplications with the tight-binding structure constants.[7,9,17]

For the *Hamiltonian matrix* one finds

$$\begin{aligned} \mathcal{H} &\equiv \langle \underline{\chi} | - \Delta + V(\mathbf{r}) | \underline{\chi} \rangle \\ &= h(1 + oh) + \langle \underline{\chi} | \varepsilon_\nu | \underline{\chi} \rangle + \langle \underline{\chi} | V_{\mathrm{NMT}}(\mathbf{r}) | \underline{\chi} \rangle. \end{aligned} \tag{20}$$

Here,

$$\langle \underline{\chi} | \varepsilon_\nu | \underline{\chi} \rangle \equiv (1 + ho)\varepsilon_\nu(1 + oh) + h\varepsilon_\nu ph$$

can be lumped together with the overlap matrix, provided that the matrix ε_ν commutes with all other matrices, i.e., if all $\varepsilon_{\nu R\ell}$'s have been chosen identical. $V_{\mathrm{NMT}}(\mathbf{r})$ in the last term of Eq. (20) is the difference between the full potential and the potential used to construct the LMTO set, that is,

$$V_{\mathrm{NMT}}(\mathbf{r}) \equiv V(\mathbf{r}) - \sum_R v_R(|\mathbf{r} - \mathbf{R}|),$$

TABLE II. Self-consistent potential parameters for Fe. The *spd* screening parameters $\underline{\alpha}_{\mathrm{II}}$ given in Eq. (4) were used. $s_{\mathrm{Fe}} = w = 2.662$ a.u.

Rydbergs	c	d	o^{-1}	ε_ν	$p^{-1/2}$
Fe s	−0.306	0.159	−2.12	−0.474	5.1
Fe p	0.330	0.0671	−1.73	−0.325	6.6
Fe d	−0.189	0.0154	1.78	−0.263	0.80

is the full potential in the interstitial region and the nonspherical part inside the spheres.

In the *atomic-sphere approximation* (ASA) the interstitial region and the nonspherical part of the potential are supposed to vanish so that, in each of the expressions (19) and (20) for the overlap and Hamiltonian matrices, the last term is neglected. The ASA is a reasonable approximation provided that there are very few electrons in the interstitial region or that the touching muffin-tin spheres can be substituted by "space-filling" atomic spheres, i.e., atomic Wigner-Seitz spheres, whose overlap does not exceed 20% (i.e., if $s_R + s_{R'} \leq 1.20|\mathbf{R} + \mathbf{R}'|$). This substitution is possible for closely packed materials, as well as for those open structures which, through the addition of interstitial spheres, can be closely packed.

The so-called combined correction for the ASA includes the last term of the overlap matrix exactly, and it includes the last term of the Hamiltonian matrix in the approximation:

$$\langle \chi_{RL}|V_{\rm NMT}(r)|\chi_{R'L'}\rangle \approx \langle \kappa_{RL}|\kappa_{R'L'}\rangle V_{\rm NMT}(RL,R'L'), \tag{21}$$

where $V_{\rm NMT}(RL,R'L')$ is some simple estimate of the non-ASA part of the potential in the region where the two orbitals overlap. For TB orbitals, this region is localized so that the estimate can be quite reliable.

The overlap matrix given in Eq. (19) is dominated by the first term. For use with the recursion method, it is therefore convenient to transform to the so-called *nearly Löwdin-orthonormalized* set,

$$|\underline{\chi}^\gamma\rangle = |\underline{\chi}\rangle(1+oh)^{-1}. \tag{22}$$

In this basis, the overlap and Hamiltonian matrices take the following simple forms:

$$\mathcal{O}^\gamma = 1 + h^\gamma p h^\gamma + \langle \underline{\kappa}^\gamma|\underline{\kappa}^\gamma\rangle, \tag{23}$$

and

$$\begin{aligned}\mathcal{H}^\gamma &= \varepsilon_\nu + h^\gamma + h^\gamma \varepsilon_\nu p h^\gamma + \langle \underline{\chi}^\gamma|V_{\rm NMT}(\mathbf{r})|\underline{\chi}^\gamma\rangle \\ &= H^\gamma + h^\gamma \varepsilon_\nu p h^\gamma + \langle \underline{\chi}^\gamma|V_{\rm NMT}(\mathbf{r})|\underline{\chi}^\gamma\rangle,\end{aligned}$$

where

$$|\underline{\kappa}^\gamma\rangle \equiv |\underline{\kappa}\rangle(1+oh)^{-1} \tag{24}$$

and

$$h^\gamma \equiv (1+ho)^{-1}h = h(1+oh)^{-1}, \tag{25}$$

or, equivalently,

$$h^\gamma = h - hoh^\gamma = h - h^\gamma oh = h^\alpha - h^\alpha o^\alpha h^\alpha + \cdots. \tag{26}$$

In Eqs. (22) and (24) it may sometimes be advantageous to use $(1+oh)^{-1} = 1 - oh^\gamma$. The nearly orthonormal representation could equally well have been obtained directly from Eqs. (13)–(15), by introducing it as that representation for which all the overlap parameters vanish. The corresponding screening constants γ are thus seen to be determined by the potential parameters $D(\dot\varphi^\gamma(s))$ through

$$\gamma_{R\ell} \equiv \frac{(s_R/w)^{2\ell+1}}{2(2\ell+1)} \frac{D(\dot\varphi^\gamma_{R\ell}(s)) - \ell}{D(\dot\varphi^\gamma_{R\ell}(s)) + \ell + 1}.$$

Note that γ, like d^γ, depends on the scale constant w. The expression, equivalent to Eqs. (25) and (26), for the two-center Hamiltonian in the nearly orthonormal representation, may be obtained from (11) as

$$H^\gamma = \varepsilon_\nu + h^\gamma = c^\gamma + \sqrt{d^\gamma} S^\gamma \sqrt{d^\gamma}. \tag{27}$$

The range of this matrix, and hence that of the nearly orthonormal orbitals (10), is determined by the potential parameter γ, and Fig. 5 of Ref. 7 shows how, for bcc and fcc vanadium, the oscillations of S^γ extend to $d/w \approx 4$, i.e., to about the sixth-nearest-neighbor shell.

E. Standard potential parameters

The position parameter c^γ (16) of the nearly orthonormal representation is the second-order estimate of the energy corresponding to the boundary condition $D(\varphi(\varepsilon,s)) = -\ell - 1$. Similarly, the width parameter d^γ (17) is the first-order estimate of $\frac{1}{2}s(s/w)^{2\ell+1}\varphi(c,s)^2 \approx \frac{1}{2}w\varphi(c,w)^2$. This means that c^γ and d^γ are more insensitive to the (somewhat arbitrary) choice of ε_ν than are c^α and d^α which are merely first- and zeroth-order estimates, respectively. For tabulations, one therefore uses c^γ and d^γ or, in *standard* notation, $C \equiv c^\gamma$ and $\Delta \equiv d^\gamma$. Given tabulated values of C, Δ, and γ, one can obtain c^α, d^α, and o^α, for any choice of α, and vice versa, using the expressions

$$\frac{c^\alpha - \varepsilon_\nu}{C - \varepsilon_\nu} = \left(\frac{d^\alpha}{\Delta}\right)^{1/2} = \frac{\alpha-\gamma}{o^\alpha \Delta} = 1 + \frac{\alpha-\gamma}{\Delta}(C-\varepsilon_\nu). \tag{28}$$

For nearly all elemental, close-packed metals, the four potential parameters, C, Δ, γ, and p have been obtained from self-consistent LMTO-ASA band-structure calculations and are tabulated in Refs. 5 and 7 at the equilibrium Wigner-Seitz radii ($s \equiv w$). In the latter reference, the self-consistently calculated atomic-volume derivatives, e.g., $dC(s\equiv w)/d\ln s$, the pressure dependencies have been tabulated as well. These atomic-sphere potentials thus correspond to atomic spheres which are kept *neutral*. Alternatively, from the values of C, Δ, γ, p, and the tabulated value of the potential at the sphere, one can, using Eqs. (205)–(207) of Ref. 7, find the atomic-volume derivatives, denoted $\delta/\delta\ln s$, of the potential parameters corresponding to *frozen* atomic-sphere *potentials*. The difference between these two types of derivatives, $d/d\ln s$ and $\delta/\delta\ln s$, expresses the importance of self-consistency in the elemental solid.

Although computed for crystalline phases, the potential-parameter tables in Ref. 7 may be used to estimate the potential parameters for noncrystalline phases. This is simpler than performing charge-self-consistent recursion-method calculations of the type that we shall describe later. If the noncrystalline phase is *monatomic*, the tabulated parameters should merely be extrapolated to the proper density (i.e., $s_X \equiv w_X \rightarrow s_{\text{non-}X} \equiv w_{\text{non-}X}$)

using the tabulated self-consistent atomic-volume derivatives, $d/d\ln s$, which hold for radius deviations of about $\pm 5\%$. In case the noncrystalline structure is so open that there are spheres which overlap by more than 20%, one should, after the extrapolation to the proper density ($w_{\text{non-}X}$), choose a new $s_{\text{non-}X}$ ($< w_{\text{non-}X}$) in such a way that the overlap is now 20% or less. The corresponding extrapolation of the potential parameters to the smaller radius ($s_{\text{non-}X}$) should be performed using the frozen-potential derivatives ($\delta/\delta \ln s$). Subsequently, Δ and γ should be multiplied by the factor $(s_{\text{non-}X}/w_{\text{non-}X})^{2\ell+1}$ in order to take into account that w no longer equals s, but the average Wigner-Seitz radius given by (8). The parameters of the two-center tight-binding Hamiltonian may finally be calculated using Eq. (28) with $\alpha = \alpha_{\text{II}}$.

Due to charge transfer, it is harder to estimate the potential parameters of an *intermetallic alloy* but, if it is possible to fill space with slightly overlapping atomic spheres whose sizes do not deviate grossly from those of the constituent metals, that is, if Vegard's law holds approximately, then one can usually assume that the spheres are sufficiently neutral that the above-mentioned construction works.[9] Otherwise, a charge-self-consistent calculation for the noncrystalline material seems to be needed. Recent experience with estimation of potential parameters for substitutionally disordered alloys is described in Ref. 21.

F. Hamiltonian for the recursion method

The Hamiltonian in the *completely orthonormal representation*,

$$\begin{aligned} |\underline{\chi}\rangle\mathcal{O}^{-1/2} &\equiv |\underline{\chi}\rangle(1+oh)^{-1}(\mathcal{O}^{\gamma})^{-1/2} \\ &= |\underline{\chi}\rangle(1-oh^{\gamma})(\mathcal{O}^{\gamma})^{-1/2} \\ &= |\underline{\chi}^{\gamma}\rangle(\mathcal{O}^{\gamma})^{-1/2}, \end{aligned} \tag{29}$$

is

$$\mathsf{H} \equiv \mathcal{O}^{-1/2}\mathcal{H}\mathcal{O}^{-1/2} = (\mathcal{O}^{\gamma})^{-1/2}\mathcal{H}^{\gamma}(\mathcal{O}^{\gamma})^{-1/2}. \tag{30}$$

In the ASA, and to third order in $h^{\gamma}p^{1/2}$ this may be expressed as

$$\begin{aligned} \mathsf{H} = H^{\gamma} &+ (h^{\gamma}\varepsilon_{\nu}ph^{\gamma} - \tfrac{1}{2}h^{\gamma}ph^{\gamma}\varepsilon_{\nu} - \tfrac{1}{2}\varepsilon_{\nu}h^{\gamma}ph^{\gamma}) \\ &-(\tfrac{1}{2}h^{\gamma}ph^{\gamma}h^{\gamma} + \tfrac{1}{2}h^{\gamma}h^{\gamma}ph^{\gamma}) + \cdots, \end{aligned} \tag{31}$$

where the only nondiagonal matrix is h^{γ}. The term in the first parenthesis is of second order in $h^{\gamma}p^{1/2}$ and of first order in the fluctuation of the ε_{ν}'s, that is, effectively, of third order in the deviation of the energy from the average ε_{ν}. We thus realize that $H^{\gamma} \equiv \varepsilon_{\nu} + h^{\gamma}$ *equals the Hamiltonian* H *to second order.* If we now use the power series (26) for h^{γ} in terms of h, we see that *the general-representation two-center Hamiltonian,* H^{α} in (11), *equals the Hamiltonian* H *to first order.* Although H^{α} equals H to first order for any choice of α for which no o^{α} parameter diverges, the energy range over which the eigenvalues and eigenvectors of the two-center Hamiltonian are useful approximations to those of H, of course depends on the values of the o^{α} parameters and, hence, on the chosen representation, α.

The *recursion method* operates with either a non-Hermitian matrix $\mathcal{O}^{-1}\mathcal{H}$ or with the Hamiltonian, $\mathsf{H} \equiv \mathcal{O}^{-1/2}\mathcal{H}\mathcal{O}^{-1/2}$, in the completely Löwdin-orthonormalized basis. With LMTO's, the latter matrix is as easily obtained as the former and, since Green's functions derived from a Hermitian matrix are simpler to deal with than those derived from a non-Hermitian matrix, then we use H. This we write as

$$\begin{aligned} \mathsf{H} = H^{\gamma} &+ [\,\langle\underline{\chi}^{\gamma}|V_{\text{NMT}}(\mathbf{r})|\underline{\chi}^{\gamma}\rangle - \tfrac{1}{2}\langle\underline{\kappa}^{\gamma}|\underline{\kappa}^{\gamma}\rangle H^{\gamma} \\ &-\tfrac{1}{2}H^{\gamma}\langle\underline{\kappa}^{\gamma}|\underline{\kappa}^{\gamma}\rangle)] + \cdots \end{aligned} \tag{32}$$

including now the term $\langle\underline{\kappa}^{\gamma}|\underline{\kappa}^{\gamma}\rangle$ in the overlap matrix (23) to first order. The energy deviations defined in connection with expression (31) are included explicitly to second order. For an infinite noncrystalline solid or liquid, H must in principle be generated in the following way: First, we use *tight-binding* structure constants, S^{α} from Eq. (7), to construct a two-center tight-binding Hamiltonian, h^{α} from Eq. (11), an interstitial overlap matrix,[17] $\langle\underline{\kappa}^{\alpha}|\underline{\kappa}^{\alpha}\rangle$, and the non-ASA term of the Hamiltonian $\langle\underline{\chi}^{\alpha}|V_{\text{NMT}}|\underline{\chi}^{\alpha}\rangle$ in a representation of tight-binding LMTO's. Then, the second-order Hamiltonian h^{γ} is obtained from the power series in Eq. (26) and $\langle\underline{\kappa}^{\gamma}|\underline{\kappa}^{\gamma}\rangle$ and $\langle\underline{\chi}^{\gamma}|V_{\text{NMT}}|\underline{\chi}^{\gamma}\rangle$ are obtained using the transformation (22). These expressions are finally substituted in (32), thus yielding H *as a power series in the two-center tight-binding Hamiltonian* h^{α}.

The matrix actually used in the recursion calculation is some truncation of H. It should be noted that not only can the matrix inversions required to obtain the *exact* matrices h^{γ} and $(\mathcal{O}^{\gamma})^{-1/2}$ not be performed for an infinite noncrystalline structure, but these matrices are also not wanted because they cannot be stored in the computer due to their long range. The power series may, however, be truncated at the point where, over the energy-range required (e.g., the range of the occupied valence bands), the accuracy is sufficient.[22] In practice, we have found it possible, with suitable choices of the ε_{ν}'s and the tight-binding representation,[18] to truncate already after the first- or, in a few cases, after the second-order terms in h^{α}. Moreover, we use the ASA, possibly with the combined correction (21). The useful result is therefore[23]

$$\begin{aligned} \mathsf{H} = H^{\alpha} - h^{\alpha}o^{\alpha}h^{\alpha} &+ (\,\langle\underline{\kappa}^{\alpha}|\underline{\kappa}^{\alpha}\rangle V^{\alpha}_{\text{NMT}} - \tfrac{1}{2}\langle\underline{\kappa}^{\alpha}|\underline{\kappa}^{\alpha}\rangle H^{\alpha} \\ &-\tfrac{1}{2}H^{\alpha}\langle\underline{\kappa}^{\alpha}|\underline{\kappa}^{\alpha}\rangle) + \cdots, \end{aligned} \tag{33}$$

where we often drop one or both of the last two terms.[24]

G. Charge density

As was mentioned above, with the recursion method we can compute one of the two Green's-function matrices, $(\varepsilon + i0^{+} - \mathsf{H})^{-1}$ or $(\varepsilon + i0^{+} - \mathcal{O}^{-1}\mathcal{H})^{-1}$, and the corresponding expressions for the charge density per energy range are

$$\begin{aligned} &N(\varepsilon,\mathbf{r}) \\ &\quad = -\pi^{-1}\,\mathrm{Im}\,\mathrm{Tr}\langle\mathbf{r}|\underline{\chi}\rangle\mathcal{O}^{-1/2}(\varepsilon + i0^{+} - \mathsf{H})^{-1}\mathcal{O}^{-1/2}\langle\underline{\chi}|\mathbf{r}\rangle \\ &\quad = -\pi^{-1}\,\mathrm{Im}\,\mathrm{Tr}\langle\mathbf{r}|\underline{\chi}\rangle(\varepsilon + i0^{+} - \mathcal{O}^{-1}\mathcal{H})^{-1}\mathcal{O}^{-1}\langle\underline{\chi}|\mathbf{r}\rangle. \end{aligned} \tag{34}$$

To calculate the charge density $n(\mathbf{r})$ which is the integral of $N(\varepsilon,\mathbf{r})$ up to the Fermi energy, we must therefore be able to evaluate either the completely orthogonal orbitals $|\underline{\chi}\rangle\mathcal{O}^{-1/2}$, or both $|\underline{\chi}\rangle$ and $|\underline{\chi}\rangle\mathcal{O}^{-1}$, in $\mathbf{r}$ space and to perform the RL summations implied in Eq. (34). For a given $\mathbf{r}$ these summations can only be performed if the orbitals have short range, and this is generally not the case for $|\underline{\chi}\rangle\mathcal{O}^{-1/2}$, and hardly for *both* $|\underline{\chi}\rangle$ and $|\underline{\chi}\rangle\mathcal{O}^{-1}$ either. With LMTO's, the expression for $\mathcal{O}^{-1/2}$ is simpler than that for $\mathcal{O}^{-1}$, as may be realized from Eqs. (19), (29), and (23), so in the following we shall stick to the first expression in Eq. (34) and discuss how the problem posed by the long range of the Löwdin-orthogonalized orbitals $|\underline{\chi}\rangle\mathcal{O}^{-1/2}$ may be circumvented. The density-of-states matrix obtained with the recursion method is thus

$$\mathsf{N}(\varepsilon) = -\pi^{-1}\mathrm{Im}\,\mathrm{Tr}(\varepsilon + i0^+ - \mathsf{H})^{-1} = \sum_j \mathsf{u}_j\delta(\varepsilon-\varepsilon_j)\underline{u}_j^\dagger, \tag{35}$$

with H given by Eq. (31) and where, in the last expression, we have transformed to the eigenrepresentation, so that the energies ε_j, the column vectors $\underline{u}_j$, and the row vectors $\underline{u}_j^\dagger$ satisfy

$$\mathsf{H}\,\underline{u}_j = \underline{u}_j\varepsilon_j, \underline{u}_j^\dagger\underline{u}_{j'} = \delta_{jj'}, \text{ and } \sum_j \underline{u}_j\underline{u}_j^\dagger = 1.$$

1. Second-order Hamiltonian

We first consider the case where $\mathsf{H} \equiv H^\alpha - h^\alpha o^\alpha h^\alpha \approx H^\gamma$, that is, where the density-of-states matrix (35) has been obtained from Eq. (33) without the combined correction for the ASA. The linear combination of nearly orthogonal orbitals specified by an eigenvector of H^γ may, using Eqs. (10) and (24), be written as

$$|\underline{\chi}^\gamma\rangle\underline{u}_j = [|\underline{\varphi}\rangle + |\underline{\dot\varphi}^\gamma\rangle(\varepsilon_j-\varepsilon_\nu)]\underline{u}_j + |\underline{\kappa}^\alpha\rangle[1-o^\alpha(\varepsilon_j-\varepsilon_\nu)]\underline{u}_j, \tag{36}$$

because $\underline{u}_j$ *diagonalizes* $h^\gamma + \varepsilon_\nu$. This means that, inside each sphere, the multicenter expansion on the left-hand side of Eq. (36) can be expressed by a single-center partial-wave expansion. In the approximation that $\mathcal{O}^\gamma \approx 1$, this "LMTO tail-cancellation condition"[5,7,9] thus leads to the following *one-center expansion* of the energy-resolved charge density in the sphere at $\mathbf{R}$:

$$N(\varepsilon,\mathbf{r}) \approx \sum_\ell\sum_{\ell'} \varphi_{R\ell}(\varepsilon,r_R)\varphi_{R\ell'}(\varepsilon,r_R) \times \sum_m\sum_{m'} Y_L(\hat{\mathbf{r}}_R)\mathsf{N}_{RL,RL'}(\varepsilon)Y^*_{L'}(\hat{\mathbf{r}}_R). \tag{37}$$

Here, $\mathbf{r}_R \equiv \mathbf{r}-\mathbf{R}$ and the radial functions $\varphi(\varepsilon,r)$ are given by the first *two* terms of the Taylor series for the partial wave normalized to unity in the sphere for all energies [see Eq. (12)]:

$$\varphi(\varepsilon,r) \equiv \varphi(r)+\dot\varphi^\gamma(r)(\varepsilon-\varepsilon_\nu)+\ddot\varphi^\gamma(r)(\varepsilon-\varepsilon_\nu)^2/2+\cdots. \tag{38}$$

Hence, the charge density $n(\mathbf{r})$ may be expressed in terms of the zero, first, and second energy moments of the on-site elements of the density-of-states matrix in the orthonormal representation $\mathsf{N}(\varepsilon)$.

The wave functions in Eq. (36) are only orthonormal in the ASA, and to first order in $h^\gamma p^{1/2}$, but the latter restriction is easily released by using for $\varphi(\varepsilon,r)$ the Taylor series (38) to *second* order,[25] and truncating the product $\varphi(\varepsilon)\varphi(\varepsilon)$ after the terms of order $(\varepsilon-\varepsilon_\nu)^2$. This procedure consistently uses basis functions which are correct to the same order as the Hamiltonian.

Self-consistent calculations in the ASA merely require the spherical average of the charge density, and this is given by the *diagonal* elements of $\mathsf{N}(\varepsilon)$, which are particularly easy to evaluate with the recursion method. The charge density, spherically averaged inside the sphere at $\mathbf{R}$ is thus

$$n_R(r_R) = (4\pi)^{-1}\sum_\ell\{\varphi(r)^2n^{(0)} + 2\varphi(r)\dot\varphi^\gamma(r)n^{(1)} + [\dot\varphi^\gamma(r)^2 + \varphi(r)\ddot\varphi^\gamma(r)]n^{(2)}\}_{R\ell}, \tag{39}$$

with the moments

$$n^{(q)}_{R\ell} \equiv \int^{\varepsilon_F} d\varepsilon(\varepsilon-\varepsilon_{\nu R\ell})^q\sum_m \underline{N}_{R\ell m,R\ell m}(\varepsilon). \tag{40}$$

One normally tries to chose each $\varepsilon_{\nu R\ell}$ at the center of gravity of the occupied part of the $R\ell$-projected band, i.e., such that the first moment in Eq. (40) vanishes.

The charge density may also be expressed as a multicenter expansion[8]

$$n(\mathbf{r}) = \sum_{R,L}\sum_{R',L'}\chi^\alpha_{RL}(\mathbf{r}-\mathbf{R})n^\alpha_{RL,R'L'}\chi^{\alpha*}_{R'L'}(\mathbf{r}-\mathbf{R}'), \tag{41}$$

in terms of the tight-binding LMTO's. Since $|\underline{\chi}^\gamma\rangle = |\underline{\chi}^\alpha\rangle(1-o^\alpha h^\gamma)$, the density-of-states matrix in the tight-binding representation is $[1-o^\alpha(\varepsilon-\varepsilon_\nu)]\mathsf{N}(\varepsilon)[1-o^\alpha(\varepsilon-\varepsilon_\nu)]$ and the density matrix entering in (41) is

$$n^\alpha_{RL,R'L'} \equiv \int^{\varepsilon_F} d\varepsilon[1-o^\alpha(\varepsilon-\varepsilon_\nu)]_{R\ell}\mathsf{N}_{RL,R'L'}(\varepsilon) \times[1-o^\alpha(\varepsilon-\varepsilon_\nu)]_{R'\ell'}. \tag{42}$$

This may be expressed in terms of the energy moments of $\mathsf{N}(\varepsilon)$. Expression (41) is more cumbersome to evaluate than the one-center expansion (37), because many more elements of the DOS matrix are needed, and the recursion method only yields one at a time. Similarly, the charge density in the interstitial region may in principle be obtained from Eq. (41), but it is presumably easier to continue the one-center expansion of Eq. (37) to $r_R > s_R$, despite the high angular-momentum components ($\ell,\ell' \le 4$) needed for large r_R.

In order to go beyond the ASA for the orthonormalization, we should instead of Eq. (36) use

$$|\underline{\chi}^\gamma\rangle(\mathcal{O}^\gamma)^{-1/2}\underline{u}_j \approx |\underline{\chi}^\gamma\rangle[1-\tfrac{1}{2}h^\gamma p(\varepsilon_j-\varepsilon_\nu)-\tfrac{1}{2}\langle\underline{\kappa}^\gamma|\underline{\kappa}^\gamma\rangle]\underline{u}_j$$
$$\approx \{|\underline{\varphi}\rangle[1-\tfrac{1}{2}(\varepsilon_j-\varepsilon_\nu)^2 p]+|\underline{\dot\varphi}^\gamma\rangle(\varepsilon_j-\varepsilon_\nu)\}\underline{u}_j-\tfrac{1}{2}[|\underline{\varphi}\rangle+|\underline{\dot\varphi}^\gamma\rangle(\varepsilon_j-\varepsilon_\nu)][1-o^\alpha(\varepsilon_j-\varepsilon_\nu)]\langle\underline{\kappa}^\alpha|\underline{\kappa}^\alpha\rangle$$
$$\times[1-o^\alpha(\varepsilon_j-\varepsilon_\nu)]\underline{u}_j+|\underline{\kappa}^\alpha\rangle[1-o^\alpha(\varepsilon_j-\varepsilon_\nu)]\underline{u}_j, \quad (43)$$

where the last approximation has the virtues of yielding a computable expression and the correct normalization. As regards the first term, we have already seen that, for the ASA, the correct orthogonalization may be obtained by substituting the wave function in the curly brackets by the second-order Taylor series (38). The last term in Eq. (43) gives rise to the interstitial charge density, and the second term is caused by the renormalization due to the integral over the interstitial region. In the simplest approximation, where we drop all energy dependencies and only renormalize the spherical part of the charge density, this second term is

$$\Delta n_R(r_R)=(4\pi)^{-1}\sum_\ell \varphi_{R\ell}(r_R)^2\sum_m\sum_{R'',L''}\langle\kappa^\alpha_{RL}|\kappa^\alpha_{R''L''}\rangle n^{(0)}_{R''L'',RL}\ ,$$

where $n^{(0)}$ is the integral up to the Fermi level of the density-of-states matrix $\mathsf{N}(\varepsilon)$.

We finally consider the case where the Hamiltonian H includes the combined correction to the ASA, i.e., where the density-of-states matrix has been obtained from the full expression (33). In that case $\underline{u}_j$ no longer diagonalizes H^γ exactly, and there is no exact tail cancellation. The charge density would thus have to be expressed by a multicenter tight-binding expansion like Eq. (41) but with the density matrix

$$n^\alpha=(1-o^\alpha h^\alpha)\left(\int^{\varepsilon_F}d\varepsilon\,\mathsf{N}(\varepsilon)\right)(1-h^\alpha o^\alpha),$$

in the approximation $\mathcal{O}^\gamma\approx 1$. Since very many matrix elements of $\mathsf{N}(\varepsilon)$ are required in this matrix product, we recommend being pragmatic and using the formulas derived under the condition of tail cancellation.

2. *First-order Hamiltonian*

The recursion to yield $\mathsf{N}(\varepsilon)$ is often carried out using from Eq. (33) only the two-center tight-binding Hamiltonian, i.e., $\mathsf{H}\equiv H^\alpha$. In this case the energies are only correct to first order and, for constructing the charge density, one should use radial functions Eq. (38) whose energy dependencies are consistent with those of the densities of states. Straightforwardly, one would truncate the Taylor series for the radial charge densities after the first-order terms, but this spoils the positive definiteness of each radial charge density and may occasionally, when the energy is far from the respective ε_ν, lead to a negative partial charge density. We therefore prefer keeping the second-order Taylor series for the radial functions and then correct the energy argument so as to keep the energy-dependent shape of each radial function consistent with that of the band (e.g., for an unhybridized band the wave function must change from bonding to antibonding when the energy changes from the bottom to the top of the band). The formalism to be compared with Eq. (36) and onwards is then as follows.

The wave function is

$$|\underline{\chi}^\gamma\rangle(\mathcal{O}^\gamma)^{-1/2}\underline{u}_j=(|\underline{\varphi}\rangle+|\underline{\dot\varphi}^\gamma\rangle h^\gamma)\underline{u}_j+|\underline{\kappa}^\alpha\rangle(1-o^\alpha h^\gamma)\underline{u}_j$$

to first order in h^γ. Since $\underline{u}_j$ now diagonalizes the two-center tight-binding Hamiltonian H^α, and not $H^\gamma=H^\alpha-h^\alpha o^\alpha h^\alpha+\cdots$, tail cancellation occurs merely to first order in h^α. We shall use the approximation

$$H^\gamma\underline{u}_j\approx\varepsilon^\gamma(\varepsilon_j)\underline{u}_j,$$

where ε_j are the eigenvalues of $\mathsf{H}\equiv H^\alpha$, and $\varepsilon^\gamma(\varepsilon)$ is defined to be a diagonal matrix with the elements

$$\varepsilon^\gamma_{R\ell}(\varepsilon)\equiv\varepsilon-(\varepsilon-\varepsilon_{\nu R\ell})^2 o^\alpha_{R\ell}\ .$$

$\varepsilon^\gamma_{R\ell}(\varepsilon)$ is thus the energy to second order, neglecting hybridization effects. This approximate treatment of the second-order effects on the wave functions enables us to use the procedures of the previous subsection to enforce orthonormality. The energy argument ε of the radial function in Eq. (38), but not that of $\mathsf{N}(\varepsilon)$, should thus be substituted by $\varepsilon^\gamma(\varepsilon)$. In Eqs. (40) and (42) $\varepsilon-\varepsilon_\nu$ should be substituted by $\varepsilon^\gamma(\varepsilon)-\varepsilon_\nu$.

The two-center tight-binding Hamiltonian (11) only depends on the potential via the values and radial derivatives at the sphere boundary of the radial wave functions; the first and second energy derivatives do not enter in the expressions (16) and (17) for the potential parameters c and d. For constructing the charge density, one may therefore prefer to avoid computation of second energy-derivative functions, at the cost of second-order nonorthogonalities, by using in Eq. (37)

$$\varphi(\varepsilon,r)=\varphi(r)[1-\tfrac{1}{2}(\varepsilon-\varepsilon_\nu)^2 p]$$
$$+\dot\varphi^\gamma(r)(\varepsilon-\varepsilon_\nu)[1-(\varepsilon-\varepsilon_\nu)o^\alpha]. \quad (44)$$

This result can be obtained from the first term of Eq. (43). The spherical average of the charge density is thus given by

$$n_R(r_R)=(4\pi)^{-1}\sum_\ell\{\varphi(r)^2 n^{(0)}+2\varphi(r)\dot\varphi^\gamma(r)n^{(1)}$$
$$+[\dot\varphi^\gamma(r)^2-2\varphi(r)\dot\varphi^\gamma(r)o$$
$$-\varphi(r)^2 p]n^{(2)}\}_{R\ell}, \quad (45)$$

in terms of the zero, first, and second energy moments (40) of the diagonal elements of $-\pi^{-1}\mathrm{Im}(\varepsilon+i0^+-H^\alpha)^{-1}$.

H. Self-consistent potential

In density-functional band-structure calculations with the LMTO method it is customary to achieve self-consistency only for the spherically-symmetric part of the charge density and in the ASA. Despite this approximation, the full charge density not made spherical obtained as the result of solving Schrödinger's equation (possibly including the combined correction) for this ASA potential has been found highly accurate,[8] and so have the total energies calculated from it.[26] Due to its simplicity, this is the self-consistency procedure that we recommend be followed also for disordered solids and liquids. The potential for the first iteration towards self-consistency is usually obtained from superposed atomic charge densities,[27] or from the elemental solids as described at the end of Sec. II E, and the following potentials are then constructed as follows.

Given an ASA charge density from a recursion calculation, the Hartree plus exchange-correlation potential is

$$v_R(r) = \int_{s_R} \frac{2n_R(r')}{|\mathbf{r}-\mathbf{r}'|} d^3r' - \frac{2Z_R}{r} + \mu_{\rm xc}(n_R(r)) - \sum_{R'\neq R} \frac{2z_{R'}}{|\mathbf{R}-\mathbf{R}'|}, \quad (46)$$

inside the sphere at $\mathbf{R}$ and in the ASA. Here $n_R(r)$ is the sum of the valence-electron density, given by Eqs. (39) or (45), and the "frozen" core-electron density obtained from an atomic calculation. The integral in the first term is in the sphere and can be reduced to the sum of two radial integrals. Z_R is the nuclear charge in that sphere. The third term is the exchange-correlation potential. The last term is the electrostatic Madelung potential, spherically averaged in the sphere, from the net nuclear minus electronic charges, $z_{R'}$, from all the other spheres. The input potential for the next recursion calculation is now a mixture of (46) and the previous potential.

The long-ranged Madelung term in Eq. (46) cannot be summed directly in the disordered structure, and the pair-correlation functions of the disordered structure have to be used. Alternatively, one may for closely packed solids use the procedure of adjusting the sphere radii s_R at each iteration step so as to keep the spheres neutral and, hence, to avoid the Madelung term.

For a two-component system like $Fe_{80}B_{20}$ we treated the Madelung potential in the following approximate way: The Madelung sum for the potential at site $\mathbf{R}$,

$$-2\sum_{R'\neq R} \frac{z_{R'}}{|\mathbf{R}-\mathbf{R}'|},$$

is approximated by the integral

$$-2\int \frac{z_1\rho_{11}(R') + z_2\rho_{12}(R')}{R'} d^3R', \quad (47)$$

for all atoms of type 1, and by

$$-2\int \frac{z_1\rho_{21}(R') + z_2\rho_{22}(R')}{R'} d^3R', \quad (48)$$

for all atoms of type 2. Here ρ_{ij} are the average, atomic, partial pair-distribution functions. We thus use the same, average Madelung potential for all atoms of the same type. To avoid cluster-size effects and slow convergence of the integrals, we multiply the pair-distribution functions by a damping factor such that for large distances (shorter than the dimension of the cluster) ρ_{ij} tends towards the partial density of the j component N_j/V, with V being the volume containing N_j atoms of type j.

I. Density-functional total energy

For a given muffin-tin or atomic-sphere potential, $v_R(r)$, not necessarily the self-consistent one given by Eq. (46), the kinetic energy is the sum of the one-electron energies minus the potential energy:

$$T = \sum_R \left(\sum_\ell \varepsilon_{\nu R\ell} n^{(0)}_{R\ell} + n^{(1)}_{R\ell} \right) - \int_{s_R} v_R(r) n_R(r) d^3r.$$

In the ASA the total energy is simply

$$E = T + \sum_R U_R + \sum_R \sum_{R'\neq R} \frac{z_R z_{R'}}{|\mathbf{R}-\mathbf{R}'|}, \quad (49)$$

where

$$U \equiv \int_{s_R} n(r) \left(\varepsilon_{\rm xc}(n(r)) - \frac{2Z}{r} + \int_{s_R} \frac{n(r')}{|\mathbf{r}-\mathbf{r}'|} d^3r' \right) d^3r,$$

is the intrasphere interaction between the electrons, and between the electrons and the nucleus in that sphere.

Current total-energy expressions employing the charge densities not made spherical are considerably more involved than Eq. (49).[26,28,29] For calculating structural energy changes we recommend the simple frozen-potential procedure[30] which amounts to calculating the total energy difference as the change in the sum of the one-electron plus Madelung energies.

J. Recursion with terminators

The recursion method is based on work by Lanczos[31] and is essentially a method for transforming a symmetric matrix into a tridiagonal form. The application of the Lanczos method to solid-state physics problems was given by Haydock and co-workers.[1,2,32] His recursion method is a real-space method for the calculation of one diagonal element of the Green's function; its imaginary part gives the orbital-projected (or partial) density of states (PDOS).

The basic idea is to generate an orthogonal subspace of dimension n by repeated operations with the Hamiltonian matrix H on a starting vector. The starting vector corresponds to that orbital for which we wish to calculate the PDOS. If $\underline{u}_1$ denotes the starting vector, the recursion procedure which generates the orthogonal subspace $\{\underline{u}_n\}$ is as follows:

$$b_1\underline{u}_2 = \mathsf{H}\,\underline{u}_1 - a_1\underline{u}_1, \quad (50)$$

$$b_n\underline{u}_{n+1} = \mathsf{H}\,\underline{u}_n - a_n\underline{u}_n - b_{n-1}\underline{u}_{n-1}.$$

The a_n, b_{n-1} are the coefficients to orthogonalize $\mathsf{H}\,\underline{u}_n$ to the preceding vectors, $\underline{u}_n$ and $\underline{u}_{n-1}$, and b_n is the

coefficient to normalize $\underline{u}_{n+1}$ to unity.

The recursion coefficients are given by

$$a_n = \underline{u}_n^\dagger \mathsf{H}\, \underline{u}_n \tag{51}$$

and

$$b_n = \underline{u}_{n+1}^\dagger \mathsf{H}\, \underline{u}_n .$$

They describe higher-order moments of the PDOS for the initial orbital and represent the influence of increasingly remote orbitals.

The new vectors generated by the Lanczos recursion method defined in Eq. (50) generate an orthonormal set in the Krylov subspace[33] $\{\underline{u}_1, \mathsf{H}\,\underline{u}_1, \mathsf{H}^2\underline{u}_1, \ldots, \mathsf{H}^{n-1}\underline{u}_1\}$. The basic Lanczos procedure can be viewed as a Gram-Schmidt orthogonalization of the set of Krylov vectors.

The new basis is therefore generated by repeated operation with H, each operation allowing the electron to hop further from the initial orbital. This procedure is very easy to implement numerically, because we need to perform only matrix multiplications. However, some care has to be taken. Round-off errors due to finite precision computers, make possible that the new vectors generated after some iterations are not orthogonal to all the preceding ones.

In the new, orthogonal basis, which has orbital number 1 in common with the original basis, the Hamiltonian has the tridiagonal form.

$$\tilde{\mathsf{H}} = \begin{pmatrix} a_1 & b_1 & & & \\ b_1 & a_2 & b_2 & & \\ & b_2 & a_3 & b_3 & \\ & & \ddots & \ddots & \ddots \end{pmatrix} . \tag{52}$$

From the Green's-function matrix $\tilde{\mathsf{G}}(z)$ associated with $\tilde{\mathsf{H}}$,

$$\tilde{\mathsf{G}}(z) = \frac{1}{z - \tilde{\mathsf{H}}}, \tag{53}$$

the PDOS for the initial orbital is

$$\mathsf{N}_{11}(\varepsilon) = \tilde{\mathsf{N}}_{11}(\varepsilon) = -\frac{1}{\pi}\mathrm{Im}\tilde{\mathsf{G}}_{11}(\varepsilon + i0^+),$$

By using the tridiagonal form for the Hamiltonian, $\tilde{\mathsf{G}}_{11}(z)$ has a continued fraction form:

$$\tilde{\mathsf{G}}_{11}(z) = \cfrac{1}{z - a_1 - \cfrac{b_1^2}{z - a_2 - \cfrac{b_2^2}{\ddots \cfrac{}{z - a_n - T^{(n)}(z)}}}} . \tag{54}$$

We have introduced a terminator $T^{(n)}(z)$ at the nth level; this does not alter the first $2n$th moments of the PDOS. In practice, we stop the recursion after about 10 levels for s and p orbitals and after about 20 levels for d orbitals.

The transformation of H to tridiagonal form is equivalent to the transformation used in the problem of calculating the PDOS associated with the surface atom of a semi-infinite, linear chain. The physical interpretation of a terminator $T^{(n)}$, which is applied after n levels of recursion, is to substitute the remaining part of the chain, after the nth atom, by an effective medium.

The problem is now to find a closed form for the terminator $T^{(n)}(z)$. For a continuous bounded energy band, the coefficients a_n and b_n tend asymptotically to constant limits, a_∞ and b_∞, which are related to the band edges ε_B and ε_T (bottom and top of the band)[34] through

$$a_\infty = \tfrac{1}{2}(\varepsilon_T + \varepsilon_B) \quad ,$$

$$b_\infty = \tfrac{1}{2}(\varepsilon_T - \varepsilon_B) \quad .$$

Normally, for this case, one uses the "square-root terminator" which assumes that after the nth level, the coefficients remain constant and equal to their asymptotic values. The result is

$$T(\varepsilon) = \frac{\varepsilon - a_\infty - i\sqrt{4b_\infty^2 - (\varepsilon - a_\infty)^2}}{2} \quad , \tag{55}$$

which ensures that the continuum of states is in the range of $a_\infty - 2b_\infty < \varepsilon < a_\infty + 2b_\infty$.

The asymptotic values are generally not known and in practice the square-root terminator often gives spurious oscillations in the PDOS curve. This is due to the abrupt matching between the known calculated coefficients and the asymptotic ones. The most commonly used evaluation of the asymptotic values is due to Beer and Pettifor.[12]

When a gap is present, the recursion coefficients oscillate[34,35] rather than tend to an asymptotic value. The square-root terminator should therefore not be applied, and if it is used, it yields a PDOS with spurious oscillations. More sophisticated ways of terminating the continued fraction for such cases have been devised by Nex.[36,37]

Our scheme for the terminator, appropriate for a gapless situation, is based on a linearization of the continued-fraction representation of $\tilde{\mathsf{G}}_{11}(\varepsilon)$ (54). It can easily be shown[38] that in the asymptotic region, the continued fraction after the nth level $\tilde{\mathsf{G}}_{11}^{(n)}$ may be written as a Fourier series

$$\tilde{\mathsf{G}}_{11}^{(n)}(\varepsilon) - T^{(n)}(\varepsilon) = \sum_{l=0}^{\infty} e^{(-il\phi)}\delta_{2n+l} \quad , \tag{56}$$

where

$$\cos\phi = \frac{\varepsilon - a_\infty}{2b_\infty} \quad ,$$

and the δ sequence is defined as

$$\delta_{2n-1} = 2(b_\infty - b_n) \qquad \text{and} \qquad \delta_{2n} = a_\infty - a_n \quad ,$$

with the property $\delta_n \to 0$ when $n \to \infty$.

The δ sequence is known up to a certain level for given asymptotic values, if one assumes that Eq. (56) holds from the first level (n=1). The idea is now to extrapolate the δ sequence from its first known values so that it tends smoothly to zero.

The fitting was done by a least-squares procedure, assuming that after some level M all terms of the sequence are linear combinations of all preceding ones:

$$\delta_k = \sum_{j=1}^{M} c_j \delta_{k-j}, \quad k > M. \tag{57}$$

This relation is equivalent to assuming that the δ sequence can be written as follows:

$$\delta_n = \sum_{i=1}^{M} d_i z_i^n \quad , \tag{58}$$

where z_i are the roots of the following polynomial:

$$z^M - \sum_{j=1}^{M} c_j z^{M-j} = 0 \quad . \tag{59}$$

Equation (58) is the same as the one used by Allan[39] to find the best fit of the δ's.

If one uses Eq. (57) separatedly for the a and b sequences the problem is reduced to the one studied by Trias, Kiwi, and Weissmann.[40]

The procedure was implemented numerically as follows: Given $2M$ pairs of calculated recursion coefficients and a guess for (a_∞, b_∞), usually the values calculated with the Beer and Pettifor method,[12] one can solve Eq. (57) for the c_i coefficients, then check if all roots of the polynomial of Eq. (59) satisfy $|z_i| \leq 1$; if they do, one uses Eq. (57) for $k > 2M$ to extrapolate the δ sequence; if they do not, one changes a_∞ and b_∞ and repeats the procedure.

In this way we avoid spurious peaks in the PDOS due to abrupt matching of the coefficients in the continued fraction. The band edges are fairly close to the ones calculated with the Beer-Pettifor method,[12] and the integrated quantities (over the complete energy range) coincide with those calculated using the Cambridge Recursion Library of Nex.[37] Recently[41] it has been demonstrated that the relation given in Eq. (56) holds, not only in the linear case and that, in general, the δ sequence is a nonlinear function of the recursion coefficients. By using this new, more general form for $\tilde{G}_{11}^{(n)}$ (56) together with the extrapolation procedure, we get further improvements using the same information as in the linear method presented here.

III. BAND-STRUCTURE AND RECURSION CALCULATIONS FOR bcc Fe

In order to demonstrate the quality of recursion calculations we first considered a *crystal,* and compared the orbital-projected densities of states (PDOS) obtained by a standard band-structure calculation, using **k**-space sampling via the tetrahedron method, with those obtained by recursion for a finite cluster, consisting of 400 atoms coordinated further to second-nearest neighbors, and the terminator described above. Since one purpose of the present paper is to study amorphous $Fe_{80}B_{20}$, we chose the crystal to be elemental bcc Fe.

In this paper, a PDOS is defined as a diagonal element (or a partial trace) of the DOS matrix (35) in the orthonormal LMTO representation, e.g., $N_{R\ell}(\varepsilon) \equiv \sum_m \mathsf{N}_{R\ell m, R\ell m}(\varepsilon)$. Due to LMTO tail cancellation, this orthonormal-orbital PDOS is also the one entering in the one-center spherical-harmonics (partial-wave) expansion of the energy-resolved electron density in Eqs. (37)–(40).

A. First-order band-structure calculation

For the band-structure calculation, as well as for the recursion, we used the ASA and the first-order Hamiltonian H in Eq. (11). The expansion energies $\varepsilon_{\nu\ell}$ were chosen at the centers of gravity of the occupied parts of the PDOS; that is, such that the first energy moments, defined by (40) with q=1, vanish. The screening constants were those for *spd* screening given by Eq. (4).

We did not perform self-consistent calculations, but used the self-consistent potential parameters listed in Table III of Ref. 7 (these calculations included the f orbitals and employed the third-order Hamiltonian). With the help of Eqs. (28), we then transformed these standard potential parameters into the position and width parameters, c_ℓ and d_ℓ, needed in the two-center tight-binding Hamiltonian, $H = c + \sqrt{d}\, S \sqrt{d}$ in Eq. (11). These parameters are listed in Table II [together with those additional parameters that would be needed to construct the third-order Hamiltonian (31)]. The structure matrix S was generated as described in Sec. II A, by inversion of the $(15 \times 9) \times (15 \times 9) = 135 \times 135$ matrix $\alpha^{-1} - S^0$ obtained when including the 15-site cluster which contains the central site and its two first-neighbor shells.

The result of the band-structure calculation is shown in the left-hand side of Fig. 1. With our choice of the expansion energies ε_ν in the middle of the occupied part of the PDOS, these PDOS curves obtained for the first-order Hamiltonian are quite accurate for energies up to the Fermi level ($\varepsilon_F = -0.11$ Ry). This may be appreciated by comparison with any good-quality calculation for bcc iron. Figure 7 of Ref. 7, in particular, shows the PDOS for the first-, second-, and third-order LMTO Hamiltonians with the same potential and ε_ν's as used in the present paper. The unoccupied, high-energy parts of the s and p bands, however, are highly distorted, pressed down in energy. That this must occur follows from the fact that the first-order Hamiltonian has the two-center tight-binding form, and this fixes the shape of the bands to being cosinelike. For the level convergence of a recursion calculation, this narrowing of the (uninteresting part of) the *sp* band turns out to be a virtue rather than a vice.

Had we, on the other hand, been interested in the unoccupied part of the energy bands, say in the energy region around 0.4 Ry, the ε_ν's should have been chosen there and the position and width parameters, c and d, would then be different. Moreover, since in that energy region there are no d bands, the basis should not contain d LMTO's in which case *sp* screening would be more appropriate. (A basis with d LMTO's might yield ghost bands switching between the $3d$ and $4d$ bands.)

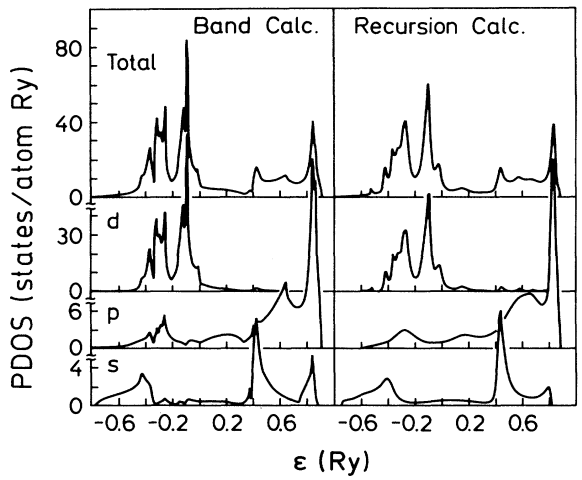

FIG. 1. PDOS curves in units of states/(atom Ry) for paramagnetic bcc Fe calculated with the first-order Hamiltonian H^{α} and *spd* screening. The left panel shows results obtained by k-space integration (Ref. 7). The results obtained using recursion with 7, 9, and 17 pairs of coefficients for the *s*, *p*, and *d* orbitals, respectively, are shown in the right-hand panel. The first-order expansion of the Hamiltonian was chosen to be around the centers of gravity of the occupied DOS. These energies are $\varepsilon_{\nu\ell} = -0.47$, -0.33, and -0.26 Ry for $\ell = s$, p, and d, respectively. The calculated Fermi level is $\varepsilon_F = -0.11$ Ry and the DOS integrated to ε_F are n_ℓ=0.83, 0.85, and 6.32 electrons per atom.

B. First-order recursion calculation

The PDOS obtained by recursion are shown in the right-hand panel of Fig. 1 and they are seen to agree rather well with the more accurate ones obtained from the band-structure calculation. The result for the recursion coefficients a_n and b_n up to level 30 for the $3d$ orbitals with t_{2g} symmetry is shown in Fig. 2. One sees that after the 20th level the coefficients corresponding to the *xy*, *yz*, and *xz* orbitals are different. This is due to the lack of cubic symmetry around the central Fe atom in our cluster of 400 atoms. We have a similar splitting after the 20th level for the e_g orbitals. The coefficients for the three *p* orbitals split already after the 13th level because the *p* orbitals are less localized than the *d* orbitals. The *n*th-level recursion coefficients are related to closed paths of length *n*, in units of the hopping range. For the evaluation of the PDOS we used 7, 9, and 17 pairs of recursion coefficients for the *s*, *p*, and *d* orbitals, respectively. These numbers ensure that the finite-size effects are negligible, and also that the symmetries are preserved.

C. Stoner model for ferromagnetic Fe

The ground state of bcc Fe is ferromagnetic with the magnetization $m = 2.2\mu_B$/atom, and this is also what standard self-consistent spin-polarized band-structure calculations give.[7] Essentially the same result is obtained if the spin-polarized band-structure is obtained from the

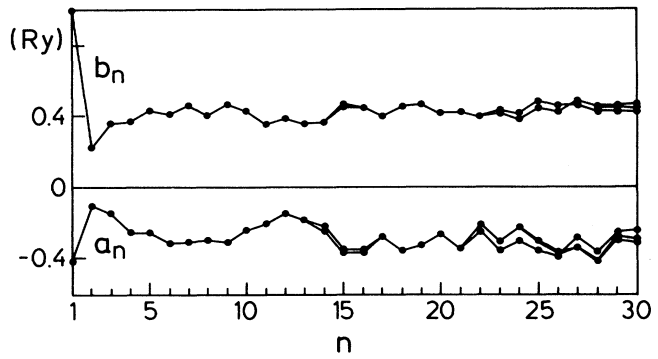

FIG. 2. The recursion coefficients a_n and b_n (Ry) for d_{xy}, d_{yz}, and d_{xz} orbitals, of the central Fe atom in the bcc cluster of 400 atoms. After $n \approx 20$ the coefficients split due to finite-size effects.

nonpolarized (paramagnetic) band structure by using first-order perturbation theory. The latter approach, with a few further approximations (see Sec. IV), leads to the generalized Stoner model[7,42] which allows one to determine the magnetization simply from the value of the Stoner parameter I and the shape of the paramagnetic DOS around the Fermi level. The latter is what we have estimated in Fig. 1, and I is an (essentially) atomic parameter which takes the value 65 mRy for Fe.[7] (This value is supposed to be used with the Fe DOS, rather than with the slightly smaller Fe *d* PDOS.)

The generalized Stoner model for an elemental ferromagnet says that the magnetization is determined by

$$I\bar{N}(m) = 1 \,, \tag{60}$$

where the function $\bar{N}(m)$ is the average of the (paramagnetic) DOS *per spin* $N(\varepsilon)$, with the average taken around the Fermi level over such an energy range that the area under the DOS is m. Explicitly, $\bar{N}(m)$ may be constructed as follows: For m given, one determines the Fermi levels $\varepsilon_F^{\uparrow}(m)$ and $\varepsilon_F^{\downarrow}(m)$ such that the two equations,

$$\tfrac{1}{2}m = \int_{\varepsilon_F^{\downarrow}}^{\varepsilon_F} N(\varepsilon)d\varepsilon = \int_{\varepsilon_F}^{\varepsilon_F^{\uparrow}} N(\varepsilon)d\varepsilon \,, \tag{61}$$

are satisfied. Then

$$\bar{N}(m) \equiv m/(\varepsilon_F^{\uparrow} - \varepsilon_F^{\downarrow}) \,. \tag{62}$$

Condition (60) is *generalized* in the sense that the usual Stoner condition, $IN(\varepsilon_F) \geq 1$, gives the condition for (weak) ferromagnetism, whereas (60) is the spin-self-consistency condition giving the value of the magnetization. A more usual way of expressing this condition is to say that the exchange splitting mI should create the magnetization m. In the following section we shall see how this Stoner model for an elemental ferromagnet may be used for the Fe_xB_{1-x} system.

Using now the DOS in Fig. 1 to estimate the magnetization, we obtain the somewhat too low value $m = 2.0\mu_B$/atom, both for the band and for the recursion calculation. The reason is our use of the first-order Hamil-

tonian, which yields a slightly wrong DOS shape around the Fermi level. Since the exchange splitting is small ($mI = 140$ mRy), the problem could have been solved by choosing expansion parameters ε_ν at the Fermi level. Alternatively, one could have used the second-order Hamiltonian.

From the generalized Stoner condition (60), we understand that the magnetization depends crucially on the crystal structure and the lattice constant, because these change the shape and the value of the DOS, respectively. Elemental Fe is a good example of this: At high pressure (> 100 kbar) Fe is hcp and has no moment. The reason is[42] that for the hcp (and fcc) structure the DOS is essentially flat near the Fermi level of Fe (but has a peak near the Fermi level of Ni). Amorphous Fe which presumably has a local structure between bcc and fcc/hcp is ferromagnetic, but with a magnetization significantly smaller than that ($2.2\mu_B$) of bcc Fe.

Since the magnetization depends so strongly on the details of the DOS around the Fermi level, some care must be taken with the terminator in the recursion method; in particular, no spurious oscillations should be allowed in this region. Recently, the recursion method was used to study magnetic properties of binary alloys.[43]

IV. BAND-STRUCTURE CALCULATION FOR CRYSTALLINE Fe_2B

As a further preliminary to our study of the electronic structure of amorphous $Fe_{80}B_{20}$, we considered crystalline Fe_2B ($\approx Fe_{67}B_{33}$), which is the simplest crystal related to $Fe_{80}B_{20}$. (Fe_xB_{1-x} crystallizes mostly in Fe_2B and pure Fe, but also Fe_3B microcrystals are present. The latter are stochiometrically closer to $Fe_{80}B_{20}$ than Fe_2B, but it has a more complicated orthorhombic structure with 16 atoms per cell.)

Fe_2B is tetragonal (a=b=5.109 and c=4.249 Å) with the Al_2Cu structure and 12 atoms per primitive cell.[44] Figure 3 shows the distribution of Fe and B atoms around an Fe atom. We performed a standard self-consistent LMTO-ASA band-structure calculation for Fe_2B including the s, p, and d LMTO's for Fe and B. The sphere sizes were chosen such as to minimize the overlap ($s_{Fe} = 2.660$ and $s_B = 2.061$ a.u.).

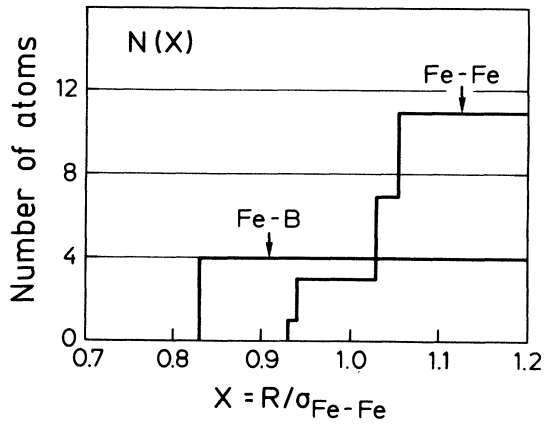

FIG. 3. Atomic distribution $N(x)$ of the Fe and B neighbors around an Fe atom in the periodic Fe_2B system (cubic Al_2Cu structure), the distance x is given in units of σ_{FeFe}=4.9057 a.u.

A. Paramagnetic electronic structure

Figure 4 shows the results for the total DOS and for the PDOS averaged over inequivalent atoms of the same kind. Also the PDOS integrated to the Fermi level, the partial occupations, are shown. The DOS has a two-peak structure which is predominantly Fe d-like and which resembles the two-peak structure in elemental Fe (Fig. 1). The latter is known to result from the bcc structure with its eight nearest and six second-nearest neighbors (fcc and hcp Fe, for instance, have a totally different DOS structure), but in Fe_2B an Fe atom is differently coordinated, as seen from Fig. 3. We shall find a similar two-peak structure in amorphous $Fe_{80}B_{20}$ and, here again, conclude that this is *not* a sign of a local bcc-like coordination.

Since the Fe sphere in Fe_2B has nearly the same size

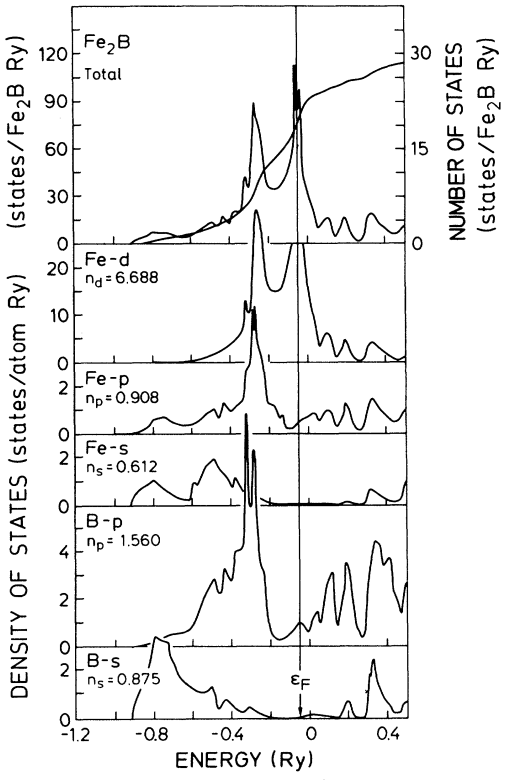

FIG. 4. PDOS and partial occupations for crystalline Fe_2B system obtained by a standard third-order LMTO-ASA band-structure calculation. For boron, only the crystalline s and p PDOS are shown, the d contribution to the occupied part of the DOS is negligible, and the number of d electrons is 0.149. In the upper panel, the DOS and the occupation curve per Fe_2B is shown.

as in elemental bcc Fe, it is meaningful to consider the self-consistent sphere charges. They are $z_{Fe} = -0.21$ and $z_B = 0.42$, and this means that electrons are transferred from B to Fe. By comparison of the partial Fe occupations with those of elemental Fe, given in the caption of Fig. 1, one may say that the 0.21 electrons transferred to Fe consist of 0.37 Fe d electrons plus 0.16 Fe sp screening holes.

B. Stoner model for Fe_xB_{1-x}

Experimentally, Fe_xB_{1-x} alloys are ferromagnetic down to $x \approx 0.4$, and like in bcc Fe their electronic structures are considerably modified due to the spin polarization. The simplest way of treating this would be with an approximation like the generalized Stoner model for the elemental ferromagnets, if possible. This will now be discussed.

In local spin-density-functional theory the perturbation felt by an up-spin–down-spin electron due to the spin polarization, $m(\mathbf{r}) \equiv n^{\uparrow}(\mathbf{r}) - n^{\downarrow}(\mathbf{r})$, is[7,42,45]

$$\Delta V_{\downarrow}^{\uparrow}(\mathbf{r}) = \pm\tfrac{1}{3}\delta(n(\mathbf{r}))\mu_x(n(\mathbf{r}))m(\mathbf{r})/n(\mathbf{r}) \tag{63}$$

to first order in $m(\mathbf{r})/n(\mathbf{r})$. The basic assumption of the Stoner model is now that this perturbation is such that it only causes spin polarization through repopulation of states at the Fermi level, and not by changing the character of occupied states (as happens, for instance, in the case of antiferromagnetism). The Stoner model thus trivially applies when the perturbation is uniform. For a real solid, where $n(\mathbf{r})$ is the density of all the electrons, $\Delta V(\mathbf{r})$ varies strongly inside any atom, but in a manner which is characteristic for that atom, because $n(\mathbf{r})$ is essentially an atomic property, and so is, to some extent, the shape of $m(\mathbf{r})$. Consequently, this variation does not necessarily invalidate the Stoner model for elemental ferromagnets where the perturbation is periodic, but not uniform, and as we know it works well for ferromagnetic $3d$ metals.

In order to proceed, let us use the ASA for $\Delta V(\mathbf{r})$. The exchange splitting of an average state at the Fermi level is, to first order and using Eq. (37) for the average state,

$$\begin{aligned}\varepsilon^{\downarrow} - \varepsilon^{\uparrow} &= \sum_R \sum_\ell \left(- \int_0^{s_r} \frac{2\delta(n_R(r))\mu_x(n_R(r))}{3n_R(r)} \frac{m_R(r)}{m_R} \varphi_{R\ell}(\varepsilon_F, r)^2 r^2 dr \right) m_R \frac{N_{R\ell}(\varepsilon_F)}{N(\varepsilon_F)} \\ &\equiv \sum_R \sum_\ell I_{R\ell}\, m_R\, \frac{N_{R\ell}}{N} \equiv \sum_R I_R\, m_R \frac{N_R}{N}.\end{aligned} \tag{64}$$

In the last line we have dropped the argument ε_F of the DOS. Moreover, we have used the definitions

$$N \equiv \sum_R N_R \equiv \sum_{R\ell} N_{R\ell}\ , \tag{65}$$

and m_R is the integral of $m_R(r)$ in the sphere.

The radial dependence of the magnetization is, under the above-mentioned assumptions, given by

$$\frac{m_R(r)}{m_R} = \sum_\ell \varphi_{R\ell}(\varepsilon_F, r)^2 \frac{N_{R\ell}(\varepsilon_F)}{N_R(\varepsilon_F)}\ , \tag{66}$$

and here, like in the last approximation in (64), we assume that for the different materials we consider, the ratios between the s, p, and d PDOS for Fe at the Fermi level do not vary much. Under this condition the Stoner parameter I is an atomic property.

We now consider the redistribution of states in the neighborhood of the Fermi level. Like in (61) and (62) we may define the energy-averaged total DOS and the energy-averaged PDOS. These satisfy

$$\begin{aligned}\bar{N}(m) \equiv m/(\varepsilon_F^{\uparrow} - \varepsilon_F^{\downarrow}) &= \sum_R m_R(m)/(\varepsilon_F^{\uparrow} - \varepsilon_F^{\downarrow}) \\ &\equiv \sum_R \bar{N}_R(m)\end{aligned} \tag{67}$$

and

$$\bar{N}_R(m) \equiv m_R(m)/(\varepsilon_F^{\uparrow} - \varepsilon_F^{\downarrow})\ , \tag{68}$$

where m is the total magnetization.

Since $\varepsilon_F^{\uparrow} - \varepsilon_F^{\downarrow}$ in Eq. (62) equals $\varepsilon^{\downarrow} - \varepsilon^{\uparrow}$ in Eq. (64), we may introduce (67) in (64). The Stoner condition for the alloy is thus

$$1 = \sum_R \bar{N}_R(m)\, \frac{N_R}{N}\, I_R. \tag{69}$$

For Fe_xB_{1-x} alloys, the B PDOS is negligible in comparison with the Fe PDOS at the Fermi level. We can therefore restrict all $\mathbf{R}$ sums to the Fe atoms. I_R is then constant and equal to I_{Fe}. With X_{Fe} being the number of Fe atoms per cell, we finally denote the average over all Fe sites by

$$\frac{1}{X_{Fe}} \sum_{R=1}^{X_{Fe}} \equiv \langle\,\rangle_{Fe} \tag{70}$$

and from now on drop all subscripts. The Stoner condition for the magnetization is thus

$$\begin{aligned}\frac{1}{I} = \langle N\bar{N}(\langle m\rangle)\rangle/\langle N\rangle &= \langle \bar{N}(\langle m\rangle)\rangle \\ &\quad + \langle \Delta N\ \Delta N(\langle m\rangle)\rangle/\langle N\rangle,\end{aligned} \tag{71}$$

here $N \equiv \langle N\rangle + \Delta N$. The condition for the ferromagnetic instability is simply

$$\frac{1}{I} \leq \langle N^2 \rangle / \langle N \rangle = \langle N \rangle [1 + \langle (\Delta N)^2 \rangle / \langle N \rangle^2] \leq \langle N \rangle \ . \tag{72}$$

The exchange splitting $\varepsilon^{\downarrow} - \varepsilon^{\uparrow}$, which is not supposed to fluctuate in the Stoner model, is

$$\varepsilon^{\downarrow} - \varepsilon^{\uparrow} = \varepsilon_F^{\uparrow} - \varepsilon_F^{\downarrow} = I\langle m \rangle = Im \ . \tag{73}$$

For an Fe_xB_{1-x} alloy, the condition for ferromagnetism is thus, to first order in the fluctuations, exactly as for elemental Fe and with the appropriate Stoner parameter and DOS being those of Fe, but averaged per Fe atom. [We remember that the DOS in the above formalism is *per spin*. If as in the figures of the present paper we use the DOS for both spins we should use $2/I$ on the left-hand sides of Eqs. (71) and (72).]

For Fe_2B we find, using $I = 65$ mRy and the DOS in Fig. 4, that the material is ferromagnetic with a magnetization of about $2\mu_B$/Fe. This is the number of states under the large DOS peak at the paramagnetic Fermi level. In the ferromagnetic phase, and in the rigid-band picture, the spin-up and spin-down average Fe PDOS, $\langle N(\varepsilon) \rangle$, are like the one shown in the figure, but with the respective Fermi levels shifted to either side of the peak. Specifically, $\varepsilon_F^{\uparrow} \approx \varepsilon_F + 70$ mRy and $\varepsilon_F^{\downarrow} \approx \varepsilon_F - 60$ mRy. Eventually, the spin-up and spin-down Fe d PDOS should, of course, be shifted in such a way that their Fermi levels are lined up. The Fe sp PDOS, and the B PDOS should be left paramagnetic.

V. RECURSION CALCULATION FOR AMORPHOUS $Fe_{80}B_{20}$

A. Structural model

We used the structural model for amorphous $Fe_{80}B_{20}$ proposed earlier by one of us.[46] This model was generated by random packing of 1500 hard spheres, and then relaxed using a truncated Morse potential. The cluster was a sphere with free boundaries. Since the experimental partial pair-correlation function shows no B-B pairs,[47] an additional constraint that two B atoms can never be closer than 1.26 times the average Fe-Fe distance was imposed.

B. Details of the calculations

1. Recursion

For the recursion, we used a cluster consisting of the 400 innermost atoms of the 1500 cluster. The size 400 is a compromise between accuracy and computer time. It seems to be sufficiently large for the innermost 50 atoms to be bulklike when using recursion with 20 pairs of coefficients for the d and 8 for the s and p orbitals. This question was addressed in the calculation for pure bcc Fe in Sec. III. The local and the site-averaged PDOS were calculated for a sample of 10 Fe and 10 B atoms randomly chosen among the 50 innermost atoms.

During the self-consistency iterations the PDOS were calculated with the usual Beer-Pettifor terminator.[12] The final PDOS were calculated with the more elaborate terminator described in Sec. II J. Both terminators gave essentially the same shape for the PDOS, but the one due to Beer and Pettifor yielded small spurious peaks near the band edges, where the more elaborate terminator gave smooth behavior. Its disadvantage is that it requires five times more computation.

2. Structure constants

First, we generated the screened structure constants $S^{\alpha}_{RL,R'L'}$, connecting each of the 400 sites (R) with its 16 nearest neighbors (R') including itself. We used *spd* screening on all Fe and B sites. When generating the structure constants by inversion of the matrix $\alpha^{-1} - S^0$ for a small cluster, as described in connection with Eq. (7), we found that the results obtained with 16-atom clusters hardly differed from those obtained with 45-atom clusters. The structure constants were finally stored as a $(400 \times 9) \times (16 \times 9)$ rectangular matrix.

3. Sphere radii

We used the ASA for simplicity, and this is presumably justified because $Fe_{80}B_{20}$ is rather closely packed. From the experimental composition and density we found the value w=2.581 a.u. for the average Wigner-Seitz radius. The radii of the Fe and B spheres used in the LMTO-ASA calculation were chosen equal to the ones used in the first ASA calculation[11] for $Fe_{80}B_{20}$; they were s_{Fe}= 2.703 a.u. and s_B=1.907 a.u. We convinced ourselves that these radii were reasonable by the following arguments. From the condition of space-filling,

$$w^3 = 0.8 s_{Fe}^3 + 0.2 s_B^3,$$

and taking the ratio s_{Fe}/s_B to be the same as between standard, tabulated atomic radii, we found the very similar radii: s_{Fe}=2.711 a.u. and s_B= 1.844 a.u. (The fact that this Fe radius was close to that of elemental bcc Fe, confirmed that the amorphous structure is, indeed, rather closely packed. Had the previous calculation not existed, we would probably have chosen the Fe sphere as in elemental bcc Fe; this would have left the size s_B= 2.191 a.u. for the B sphere.) Finally, we checked that the overlap between the spheres in the amorphous structure did not get unacceptably large. By this we mean that the linear overlap defined as $(s_1 + s_2 - d_{12})/d_{12}$ between two spheres almost never exceeds 20%. For comparison, the overlap in elemental fcc, bcc, and sc crystals, which have, respectively, 12, 8, and 6 nearest neighbors, is 10.5%, 14%, and 24%. The distribution of overlaps in the amorphous $Fe_{80}B_{20}$ cluster calculated for a sample of $\approx$ 3000 pairs of overlapping spheres is shown in Fig. 5. It is seen that, whereas the Fe-Fe overlap is satisfactory, the Fe-B overlap is only marginally so.

4. Hamiltonian

The potential parameters were calculated self-consistently for the average Fe and the average B atom

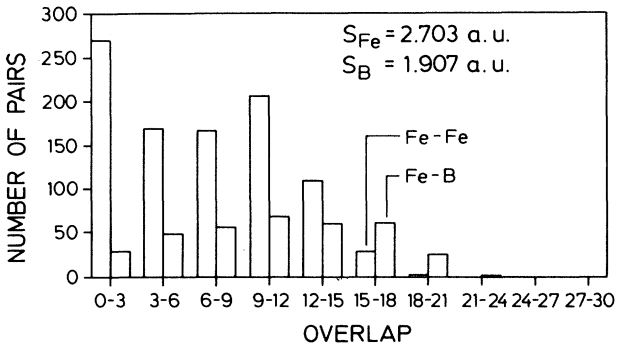

FIG. 5. Histogram showing the sphere overlap (in percent) of Fe-B and Fe-Fe pairs in amorphous $Fe_{80}B_{20}$. The overlap is defined as $(s_1 + s_2 - d_{12})/d_{12}$. Very few pairs have an overlap exceeding 20%.

by the simplest possible first-order procedure described in Sec. II F 2. The self-consistent calculations were thus performed with the Hamiltonian in Eq. (33) truncated after the first-order term, i.e., with the two-center tight-binding Hamiltonian $H \equiv c + \sqrt{d}\, S\sqrt{d} = \varepsilon_\nu + h$ from Eq. (11). The ε_ν parameters were, as usual, chosen at the centers of gravity of the occupied PDOS. The charge density was averaged over all Fe and over all B spheres, and the potential was assumed to be the same in all Fe and in all B spheres, as explained in Sec. II H. After self-consistency was achieved, the final PDOS calculations were carried out to second order, using the Hamiltonian *H-hoh* in Eq. (33).

After a preliminary calculation, which included the B *d* partial waves and the B *d* PDOS, we decided that their inclusion was not warranted. Consequently, the two-center tight-binding Hamiltonian H was truncated, such that it included only the *sp* partial waves on B, in addition to the *spd* partial waves on Fe.

C. Results

Here and in the following, the DOS is defined as $N(\varepsilon) \equiv 0.8N_{Fe}(\varepsilon) + 0.2N_B(\varepsilon)$, with $N_{Fe}(\varepsilon)$ being the Fe PDOS summed over all orbitals on an Fe site and averaged over 10 random Fe sites, and similarly for $N_B(\varepsilon)$.

1. Effects of structure-constant approximations

In Figs. 6(a)–6(c) we show the DOS calculated with the first-order Hamiltonian H, and with various approximations for the structure constants S, described in Sec. II A. In all cases the calculations were performed self-consistently, that is, a particular approximation for the structure constants was done consistently throughout all iterations. In 6(a) and 6(b) we used the interpolation formula (9), with the parameters from Table I, for the off-site (hopping) elements. The on-site elements were taken in 6(a) to be site independent, and equal to the average between the fcc and bcc values;[6,7] this is the prescription used in the original calculation.[11] In 6(b) the on-site elements were properly site dependent and calculated according to Eq. (6) by hopping to the neighbors using S^0 and hopping back using S, approximated by the interpolation formula. In 6(c) the structure matrix was calculated "properly" by inversion of the matrix $\alpha^{-1} - S^0$ for 16-atom clusters. Finally, in 6(d) the structure constants and the self-consistent potential parameters were as in 6(c), but the second-order Hamiltonian was used for the final DOS calculation.

Figure 6(a) demonstrates that the use of approximate on-site elements can lead to significant errors. In particular, the bottom of the band (B *s*-like) has developed a spurious tail and what should have been a shoulder at about −0.5 Ry (B *p*-like) has become a broad maximum at −0.7 Ry. Obviously, the B *s*- and *p*-orbital energies are too low, and the simple reason is that B does not have between 12 and 8 nearest neighbors, as assumed when taking the on-site elements as the average between fcc and bcc, but rather, 6 or less. [From tables in Refs. 6, 7, and 9 one may see, that for the sc structure, which has 6 nearest neighbors, the on-site *s*-element of the structure

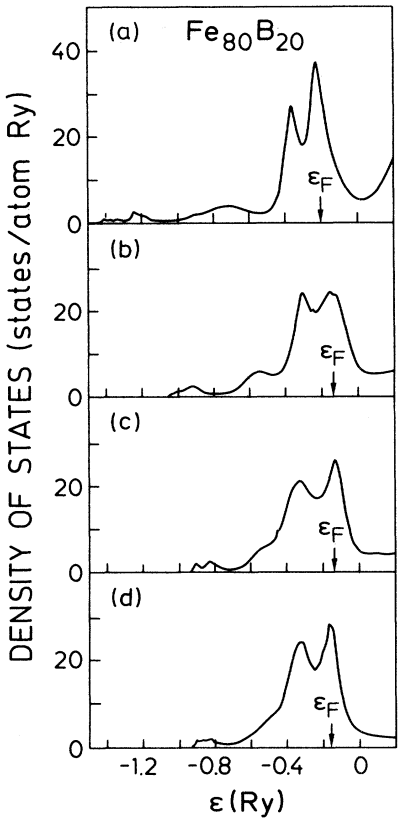

FIG. 6. DOS per atom in amorphous $Fe_{80}B_{20}$, calculated with different approximations. (a)–(c) First-order Hamiltonian. (d) Second-order Hamiltonian. The structure constants were obtained from (a) the interpolation formula for the off-site elements and the average of the bcc and fcc values for the on-site elements, (b) the interpolation formula for the off-site elements and using the Dyson equation (7) for the on-site elements, (c) and (d) exact inversion.

TABLE III. Self-consistent potential parameters for $Fe_{80}B_{20}$. The *spd* screening parameters $\underline{\alpha}_{II}$ given in Eq. (4) were used. s_{Fe}=2.703 a.u., s_B=1.907 a.u., and w=2.581 a.u.

Rydbergs	c	d	o^{-1}	ε_ν	$p^{-1/2}$
Fe s	−0.415	0.153	−1.68	−0.584	5.1
Fe p	0.172	0.0655	−1.42	−0.419	6.7
Fe d	−0.250	0.0188	1.66	−0.315	0.77
B s	−0.842	0.206	4.50	−0.763	6.8
B p	0.275	0.098	5.24	−0.455	5.6

constant is 3.72 rather than 3.05 and 3.09 for fcc and bcc, respectively. Multiplied by the potential parameter d_{Bs} = 0.2 Ry (Table III), this yields a displacement of 0.14 Ry for the B s-orbital energy.] In the self-consistent calculation, this leads B to donate too few electrons to Fe and, consequently, also to errors in the potential parameters. This is, for instance, the reason why the Fe d-like peak is too narrow and sits at too low an energy.

Proper calculation of the on-site elements, but keeping the interpolation for the hopping integrals, requires very little extra computation and, as seen in 6(b), improves the calculation considerably. The DOS is now correctly positioned and has the correct general shape. For many purposes, this is a useful approximation.

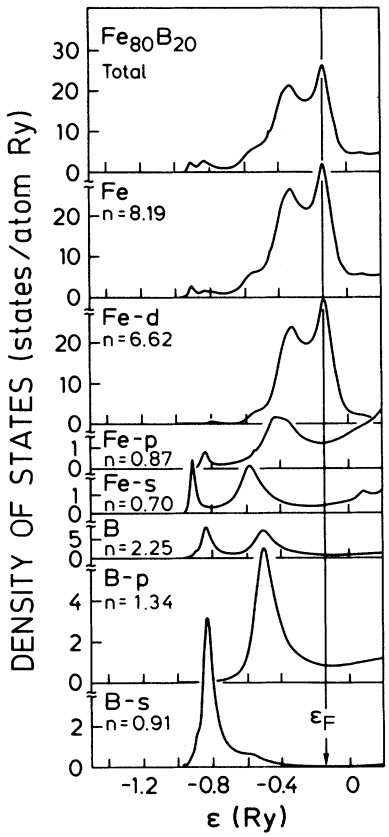

FIG. 7. Total DOS per atom, average local PDOS, and average local s, p, and d PDOS in $Fe_{80}B_{20}$ using the first-order Hamiltonian.

Calculation of the structure constants by inversion of a $\approx$ 150 × 150 matrix for each site is far more expensive than interpolation, but it improves the details of the DOS, as seen in 6(c), and is essential for the site dependence of the PDOS. We checked that the self-consistent potential resulting from the cheap approximation 6(b) is sufficiently accurate to yield a DOS like the one shown in 6(c) when used in a recursion calculation employing the proper structure constants. In other words, the difference between the DOS in 6(b) and 6(c) is due to the difference in the structure constants, rather than in the potential parameters.

The self-consistent potential parameters obtained with the first-order Hamiltonian and the inversion scheme 6(c) are given in Table III.

2. *Effects of Hamiltonian approximations*

Inclusion of the second-order correction *hoh* in the recursion is costly, because it requires one (o is diagonal) matrix multiplication and increases the range of the hopping, but as seen in 6(d) it considerably improves the states far away from ε_ν. This is seen even more clearly by comparison of the site-averaged PDOS for the first-order Hamiltonian shown in Fig. 7 with those for the second-order Hamiltonian shown in Fig. 8. Most striking is the improvement of the B s PDOS at the bottom of the band and the resulting decrease in the number of B s electrons from 0.91 to 0.61 per atom. Neglecting hybridization, the second-order correction is $-(\varepsilon-\varepsilon_\nu)^2/o^{-1}$, and this moves energies downwards when o is positive, and upwards when o is negative. From the values of o^{-1} and ε_ν in Table III one may then realize that near the bottom of the band, the visible change in the B s PDOS is mostly due to the improved description of the Fe s band with which it hybridizes; remember, there are *no* B-B nearest neighbors. [At the bottom of the band, $-(\varepsilon-\varepsilon_\nu)^2/o^{-1}$ = 60 and −4 mRy for Fe s and B s, respectively.] For energies above the Fermi level, that is, further away from the ε_ν's, the effects of the second-order correction are easy to see in Fig. 8; for the Fe s and p PDOS they are essentially as described for bcc Fe in Sec. III. Recently, Bose, Jaswal, and Andersen[14] demonstrated for the Ca_7Al_3 glass that the computationally fast approximation of including the *hoh* correction only for those hopping integrals which are already nonzero in H works surprisingly well.

For the following discussion of the electronic structure,

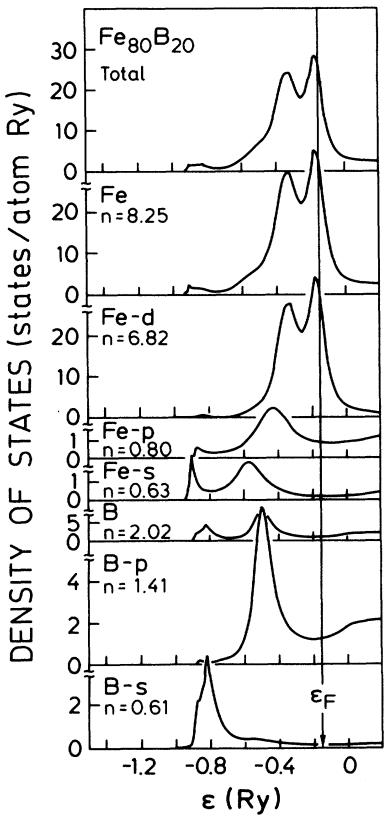

FIG. 8. As Fig. 7, but using the second-order Hamiltonian.

we shall use the results obtained with the second-order Hamiltonian.

3. Chemical binding

One of the most striking aspects of Fig. 8 is that the number of B s electrons is as small as 0.6 and the number of B p electrons as large as 1.4. Naively, one would have expected an ionic picture in which B donates its p electron to Fe and keeps its two s electrons. The picture offered by Fig. 8 is, however, a strongly *covalent* one, in which the B s PDOS is broken up into an occupied bonding part (at about −0.8 Ry on the scale of the figure) and an empty antibonding part (above the frame of the figure) due to the interaction with the Fe s and d orbitals. The large B p occupancy is coming from a strong Fe—B bond, presumably of Bp_z–Fed_{3z^2-1} character, which gives rise to the strong peak at −0.5 Ry. A somewhat similar picture was offered by Fe_2B in Fig. 4.

The charge transfer in Fig. 8 is seen to be $z_{Fe} = -0.25$ and $z_B=+1.0$. In order to illustrate the sensitivity of this number to the choice of sphere sizes, we now estimate what the charge transfer would be for Fe spheres with the same volume as in elemental Fe metal (at normal pressure). This volume is 4.6% smaller and the corresponding reduction in the number of electrons may be estimated by assuming that the density on the surface of the Fe sphere is equal to the one tabulated for elemental Fe in Table V of Ref. 7. This tabulation gives this density times the atomic volume (i.e., the number of "free" electrons) as 3.06 electrons/Fe. The reduction is therefore 0.14 electrons/Fe and the resulting charge transfer is thus $z_{Fe} = -0.11$ and $z_B=+0.44$. In conclusion, the electron transfer *is* from B to Fe, but it is not large, and it is similar to what we found in Fe_2B.

That the potential in the Fe sphere is not very different from the one in elemental Fe can be seen by comparison of the Fe potential parameters in Tables II and III. Considering the differences in the radii and in the order of the Hamiltonians used, the only significant difference in the potential parameters is a downwards Madelung shift by less than 0.1 Ry in $Fe_{80}B_{20}$. This shift is small compared with the bandwidths in Fig. 8 and the simple neutral-atomic-sphere estimation of potential parameters,[9] which simply takes the ones tabulated for the elements, would therefore hold quite well.

This analysis supports our conclusion that the bonding in $Fe_{80}B_{20}$ is predominantly covalent between Fe and B, and metallic between the irons.

4. Paramagnetic electronic structure

Our DOS in Fig. 8 exhibits a B s-related maximum 9 eV below the Fermi level, a B p-related shoulder 5 eV below ε_F, and a pronounced double peak at 2.5 and 0.1 eV below ε_F.

A characteristic feature is the double-peak structure. This seems to have a similar origin as the double peak in Fe_2B which, in turn, we concluded is *not* related to the well-known double peak in the bcc transition metals. As we shall see, this does not seem to be the case in amorphous $Fe_{80}B_{20}$ either.

We now study the correlation between the local environment of an Fe atom and its calculated PDOS. In Fig. 9 we show for five individual Fe atoms the distribution of neighbor distances and the PDOS (as usual, per Fe atom and for both spins). These five atoms were chosen among the ten central ones, used for performing the average shown in Fig. 8, in such a way that the extreme variations in the PDOS are included. The radial distributions are seen to exhibit considerable fluctuations, and so do the PDOS. The charge z_{Fe} fluctuates around the average −0.25, from +0.24 to −0.93. In a proper calculation, which is self-consistent not only on the average, these charge fluctuations would be screened out somewhat. The correlation between a strong, low-energy PDOS tail and the existence of close B atoms is easily seen. Most, but not all, of the PDOS exhibit the Fe d double hump but we have not been able to see any correlation between this and the radial distribution functions. Therefore, the simple idea that the double-hump–rectangular PDOS shape should correlate with the bcc–fcc(hcp)-like radial distributions $(0,8,14,\ldots)/(0,12,\ldots)$, does not seem to hold.

5. Ferromagnetic electronic structure

Experimentally, amorphous Fe_xB_{1-x} is ferromagnetic for $1 \leq x \leq 0.4$. With x decreasing from 1, the magneti-

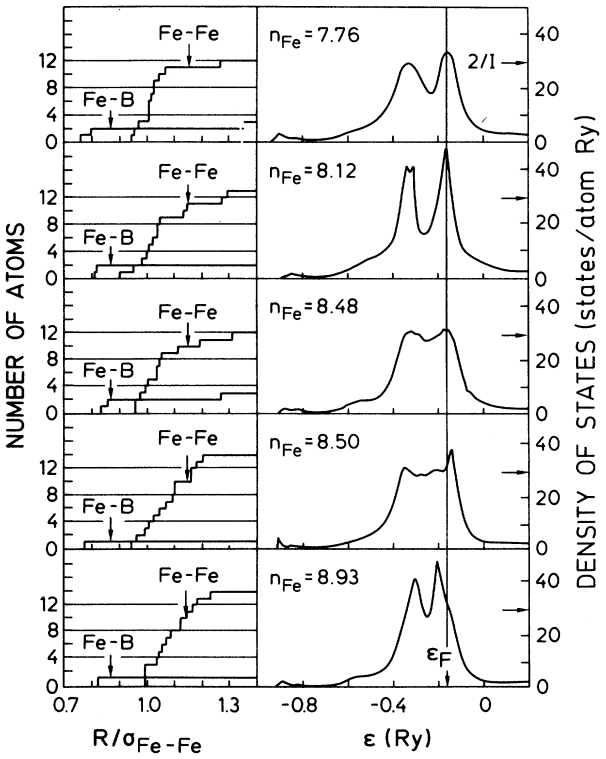

FIG. 9. Radial atomic distributions around five different Fe atoms and their PDOS. The value $2/I$ indicated on the PDOS axis relates to the Stoner criterion for the magnetic moment as given by Eqs. (71) and (73).

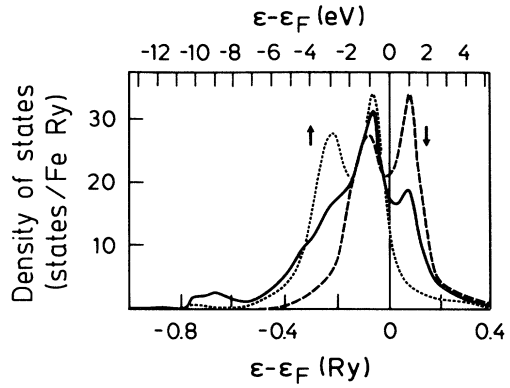

FIG. 10. Ferromagnetic total DOS for amorphous $Fe_{80}B_{20}$ (solid line), the $3d$ majority (↑) and minority (↓) PDOS for the average Fe atom are also shown (dot and dashed lines). The exchange splitting energy is $\Delta E = 143$ mRy, the Stoner parameter $I = 65$ mRy, and the average magnetization $m = 2.2\mu_B$/Fe.

zation first increases (from its value for amorphous pure Fe) to a maximum of about $2\mu_B$/Fe for $x \approx 0.8$, and thereafter it decreases. This has been originally explained as the effect of electron transfer from B to gradually fill the Fe d states.[48] More recently,[49,50] spin polarized empirical tight-binding calculations, including Coulomb correlation among Fe d electrons in amorphous Fe_xB_{1-x}, gave the correct behavior of the magnetic moment over the whole range of concentrations.

For $Fe_{80}B_{20}$ we find a magnetization of $2.2\mu_B$/Fe when we use the Stoner theory in Sec. IV B, Eqs. (71)–(73) and the average Fe PDOS, $\langle N \rangle$, from Fig. 8. [The local Fe PDOS, N, in Fig. 9 may be used to check that the second-order term in (71) is small, and to estimate the size of the moment fluctuations.] The exchange splitting of the Fe d PDOS is thus 0.14 Ry= 1.9 eV, and in Fig. 10 we show the average spin-up and spin-down Fe d PDOS together with the ferromagnetic total DOS.

The ferromagnetic DOS in Fig. 10 exhibits a strong peak 1 eV below the Fermi level. This is the coinciding upper half of the double peak for spin-up plus the lower half of the double peak for spin-down. The shoulder at −3 eV is the lower half of the spin-up double peak. Finally, like in the paramagnetic DOS, there is a shoulder at −5 eV and a peak at −9 eV which are related to bonds involving, respectively, B p and B s orbitals. This we may now compare with results of photoemission spectroscopy. The existing results scatter[51] but nearly all yield energy-distribution curves which resemble the occupied part of our DOS curve. The most recent measurement[51] found weak maxima superposed on a slowly rising edge at −5.5 and −3 eV below the Fermi level, the onset of a steep rise at −2 eV, and a flat double peak with maxima at −1 and 0 eV. This is in very close agreement with our DOS, with the possible exception that the experimental DOS at the Fermi level is higher than ours, i.e., we do not have a peak at ε_F. It was speculated that the origin of the narrow double peak was magnetic exchange splitting. This is indeed what we find and, in addition, we seem to be able to interpret the −3- and −5-eV peaks. Only one experiment[52] showed a −9-eV peak, but doubts were raised about its origin. We agree with the interpretation that it *is* the B s peak, and that the reasons why this peak was not found in other data are the small cross section for photoionization and the large lifetime broadening.

We thus believe that the double peak in the paramagnetic DOS exists, although we still do not understand its cause in terms of local bonding. This double peak was not found in a recent calculation performed with the same structural model but with a different, empirical Hamiltonian.[53]

Our value for the DOS at the Fermi level is about 15 states/(atom Ry). This is somewhat low compared with the experimental[54] electronic specific heat value of about 40 states/(atom Ry), even when taking into account electron-phonon and spin-fluctuation enhancements. (In fcc Ni, these enhancements amount to a factor of over 2, but in bcc Fe to somewhat less.)

VI. CONCLUSION

We have given a rather complete review of a method used recently for density-functional calculations for topologically disordered condensed matter. This method

combines the recursion and LMTO methods, and uses the tight-binding representation in a nontrivial way. The method can be applied at different levels of approximation but, so far, the LMTO matrix elements have always been evaluated in the atomic-sphere approximation (ASA). Various levels of approximation for this ASA Hamiltonian, such as the two-center tight-binding one, have been systematically derived and tested.

As demonstrations, we have applied the method to crystalline bcc Fe and to amorphous $Fe_{80}B_{20}$. Charge self-consistency was only treated for the average Fe and the average B atoms. For the ferromagnetic electronic structure we used a Stoner-like theory. The Fe-B bonding was found to be covalent, rather than ionic. The structures of our density of states for ferromagnetic $Fe_{80}B_{20}$ agree in detail with reliable photoemission data.

*Present address: Universidad Nacional Mayor de San Marcos de Lima, Facultad de Física, P.O. Box 454, Lima, Peru.

†Present address: University of Tokyo, Department of Applied Physics, Faculty of Engineering, Bunkyo-Ku, Tokyo 13, Japan.

[1] V. Heine, D. W. Bullett, R. Haydock, and M. J. Kelly, in *Solid State Physics*, edited by F. Seitz and D. Turnbull (Academic, New York, 1980), Vol. 35.

[2] R. Haydock, V. Heine, and M. J. Kelly, J. Phys. C **8**, 2591 (1975).

[3] F. Cyrot Lackmann, J. Phys. (Paris) Suppl. C **1**, 67 (1970).

[4] F. Yndurain, J. D. Joannopoulos, M. L. Cohen, and L. M. Falicov, Solid State Commun. **15**, 617 (1974).

[5] O. K. Andersen, Solid State Commun. **13**, 133 (1973); Phys. Rev. B **12**, 3060 (1975); in *The Electronic Structure of Complex Systems*, edited by W. Temmerman and P. Phariseau (Plenum, New York, 1984); H. L. Skriver, *The LMTO Method* (Springer, New York, 1984).

[6] O. K. Andersen and O. Jepsen, Phys. Rev. Lett. **53**, 2571 (1984).

[7] O. K. Andersen, O. Jepsen, and D. Glötzel, in *Highlights of Condensed-Matter Theory*, edited by F. Bassani, F. Fumi, and M. P. Tosi (North-Holland, New York, 1985). Due to certain pitfalls in the notation of this paper the notation was changed in the subsequent papers, Refs. 8 and 9. The latter notation is used in the present paper. The relation between the notations is as follows: $\varepsilon = \mathrm{E}$, $S^\alpha = \bar{S}$, $S^0 = S$, $\alpha = \bar{Q}$, $\gamma = Q$, $\underline{\chi}^\alpha = \underline{\bar{\chi}}$, $\underline{\chi}^\gamma = \underline{\chi}$, $\dot{\phi}^\alpha = \dot{\bar{\phi}}$, $c^\alpha = \bar{C}$, $c^\gamma = C$, $d^\alpha = \bar{\Delta}$, $d^\gamma = \Delta$, $h^\alpha = \bar{h}$, $h^\gamma = h$, $o^\alpha = \bar{o}$, $H^\alpha = \bar{H}^{(1)}$, and $H^\gamma = H^{(2)}$. In Sec. 4.8 on the combined correction to the ASA there is a minus sign missing in the first equation (115), which should read $\langle ss\sigma \rangle = -\frac{1}{2}(d/w)$. Furthemore, on the left-hand side of (120) the overbars are missing.

[8] O. K. Andersen, Z. Pawlowska, and O. Jepsen, Phys. Rev. B **34**, 5253 (1986).

[9] O. K. Andersen, O. Jepsen, and M. Sob, in *Electronic Band Structure and its Applications*, edited by M. Yussouff, Lecture Notes in Physics Vol. 283 (Springer-Verlag, Berlin, 1987).

[10] O. Gunnarsson, O. Jepsen, and O. K. Andersen, Phys. Rev. B **27**, 7144 (1983).

[11] T. Fujiwara, J. Non-Cryst. Solids **61-62**, 1039 (1984).

[12] N. Beer and D. G. Pettifor, in *The Electronic Structure of Complex Systems*, edited by P. Phariseau and W. M. Temmerman (Plenum, New York, 1984).

[13] S. K. Bose, K. Winer, and O. K. Andersen, Phys. Rev. B **37**, 6262 (1988).

[14] S. K. Bose, S. S. Jaswal, and O. K. Andersen, Phys. Rev. B **37**, 9955 (1988).

[15] S. K. Bose, J. Kudrnovsky, I. I. Mazin, and O. K. Andersen, Phys. Rev. B **41**, 7988 (1990).

[16] H. M. Petrilli and S. Frota-Pessôa, J. Phys. Condens. Matter **2**, 135 (1990); **2**, 149 (1990).

[17] M. Sob, O. Jepsen, and O. K. Andersen, Z. Phys. Chem. (Neue Folge) **157**, 515 (1988); and (unpublished).

[18] The tight-binding representations (3) and (4) are not the only ones possible. It is, for instance, not necessary that all sites have the same screening constant, and the sets obtained from either (3) or (4) in the following way: $\alpha_{\mathrm{I};R\ell} \equiv (\sigma_R/w)^{2\ell+1}\alpha_{\mathrm{I};R\ell}$, and similarly for α_{II}, generate tight-binding representations too (Refs. 9 and 17). Here, the site-dependent screening constants are specified through screening radii σ_R which may be chosen freely within the constraint that the average volume of the corresponding spheres equals the volume of the average Wigner-Seitz sphere with radius w in Eq. (8), i.e., $(1/N)\sum_{R=1}^{N}(\sigma_R/w)^3 \equiv 1$.

[19] J. C. Slater and G. F. Koster, Phys. Rev. **94**, 1498 (1954).

[20] The relation to the notation in Refs. 7 and 9 is $|\kappa^\alpha\rangle \equiv |K^\alpha\rangle^{\mathrm{i}}(2d^\alpha/w)^{1/2}$.

[21] J. Kudrnovsky, S. K. Bose, and O. K. Andersen, Phys. Rev. B **43**, 4613 (1991).

[22] An alternative to obtaining H^γ from a truncation of the series $H^\gamma = H^\alpha - h^\alpha o^\alpha h^\alpha + \cdots$, is to use (27) together with a truncation of the series $S^\gamma = S^\alpha + S^\alpha(\gamma - \alpha)S^\alpha + \cdots$, which follows from Eq. (6). This procedure does, however, not lead to a one-electron spectrum which is correct to a particular order in the deviation of the energy from ε_ν.

[23] A simpler form of the combined correction may be obtained by linearizing the general-κ KKR-ASA equations [O. K. Andersen (unpublished)]. See also Ref. 17.

[24] Note that, whereas $\langle \underline{\kappa}^\alpha | \underline{\kappa}^\alpha \rangle$ times H^α is a matrix product, $\langle \underline{\kappa}^\alpha | \underline{\kappa}^\alpha \rangle$ times V^α_{NMT} is a scalar product.

[25] The ASA tail-cancelation condition, which is essentially the KKR condition for κ=0, holds for the exact partial waves $\varphi(\varepsilon, r)$, i.e., to all orders in $\varepsilon - \varepsilon_\nu$. The proof given in Refs. 7 and 9 uses the proper energy-dependent MTO's rather than the linearized LMTO's.

[26] K. H. Weyrich, Phys. Rev. B **37**, 10 269 (1988).

[27] L. F. Mattheiss, Phys. Rev. **134**, A970 (1964).

[28] M. Sprinborg and O. K. Andersen, J. Chem. Phys. **87**, 7125 (1987); M. Methfessel, C. O. Rodriguez, and O. K. Andersen, Phys. Rev. B **40**, 2009 (1989).

[29] P. Blöchl, Ph.D. thesis, Universität Stuttgart, 1988.

[30] A. R. Mackintosh and O. K. Andersen, in *Electrons at the Fermi Surface*, edited by M. Springford (Cambridge University Press, England, 1980).

[31] C. Lanczos, J. Res. Natl. Bur. Stand. Sec. B **45**, 255 (1950).

[32] R. Haydock, in *Solid State Physics*, edited by H. Ehrenreich, F. Seitz, and D. Turnbull (Academic, New York, 1980), Vol. 35, p. 129.

[33] Given a $n \times n$ H matrix and a starting vector $\underline{u}_1$, the family of Krylov subspaces K^κ, $\kappa = 1, 2, \ldots, n$ is defined as follows: $K^\kappa = \mathrm{space}\{\underline{u}_1, \mathrm{H}\,\underline{u}_1, \mathrm{H}^2\underline{u}_1, \ldots, \mathrm{H}^{\kappa-1}\underline{u}_1\}$.

[34] J. P. Gaspard and F. Cyrot-Lackmann, J. Phys. C **6**, 3077 (1973).
[35] P. Turchi, F. Ducastelle, and G. Treglia, J. Phys. C **15**, 2891 (1982).
[36] C. M. M. Nex, J. Phys. A **11**, 653 (1978).
[37] C. M. M. Nex, Comput. Phys. Commun. **34**, 101 (1981).
[38] C. H. Hodges, J. Phys. **38**, L187 (1977).
[39] G. Allan, J. Phys. C **17**, 3945 (1984).
[40] A. Trias, M. Kiwi, and M. Weissmann, Phys. Rev. B **28**, 1859 (1983).
[41] P. Vargas, M. Weissmann, J. E. Ure, and N. Majlis, Solid State Commun. **74**, 703 (1990).
[42] U. Gunnarsson, J. Phys. F **6**, 587 (1976); O. K. Andersen, J. Madsen, U. K. Poulsen, O. Jepsen, and J. Kollar, Physica B+C **86-88B**, 249 (1977).
[43] S. Frota-Pessôa, Phys. Rev. B **36**, 904 (1987).
[44] K. Schubert, *Kristallstrukturen Zweikomponentiger Phasen* (Springer, Berlin, 1964).
[45] J. F. Janak, Phys. Rev. B **16**, 225 (1977).
[46] T. Fujiwara, H. S. Chen, and Y. Waseda, Z. Naturforsch. **37a**, 611 (1982); R. Yamamoto and M. Doyama, J. Phys. F **9**, 617 (1979).
[47] S. Steeb, S. Falch, and P. Lamparter, Z. Metallkunde **75**, 592 (1984).
[48] A. Z. Maksymowicz, T. Stobiecki, E. Jarocki, and W. Karas, Phys. Status. Solidi B **126**, 91 (1984).
[49] S. Krompiewski, U. Krey, and H. Ostermeier, J. Magn. Magn. Mater. **69**, 117 (1987).
[50] S. Krompiewski, U. Krauss, and U. Krey, Physica B **161**, 219 (1989).
[51] Th. Paul and H. Neddermeyer, J. Phys. F **15**, 79 (1985).
[52] A. Amamou and G. Krill, Solid State Commun. **33**, 1087 (1980).
[53] H. Ostermeier, Ph.D. thesis, Universität Regensburg, 1988.
[54] M. Matsuura, U. Mitzutani, and Y. Yazawa, J. Phys F **11**, 1393 (1981).